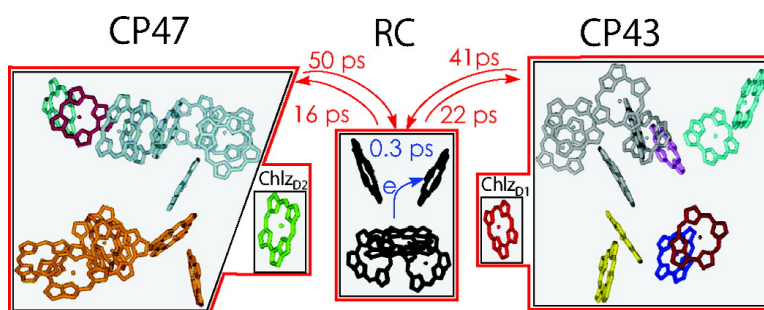**Article**

Light Harvesting in Photosystem II Core Complexes Is Limited by the Transfer to the Trap: Can the Core Complex Turn into a Photoprotective Mode?

Grzegorz Raszewski, and Thomas Renger

More About This Article

Additional resources and features associated with this article are available within the HTML version:

- Supporting Information
- Links to the 4 articles that cite this article, as of the time of this article download
- Access to high resolution figures
- Links to articles and content related to this article
- Copyright permission to reproduce figures and/or text from this article

View the Full Text HTML

Light Harvesting in Photosystem II Core Complexes Is Limited by the Transfer to the Trap: Can the Core Complex Turn into a Photoprotective Mode?

Grzegorz Raszewski and Thomas Renger*

Institut für Chemie und Biochemie (Kristallographie), Freie Universität Berlin, Fabeckstrasse 36a, 6, D-14195 Berlin, Germany

Received November 5, 2007; E-mail: rth@chemie.fu-berlin.de

Abstract: A structure-based modeling and analysis of the primary photophysical reactions in photosystem II (PS-II) core complexes is presented. The modeling is based on a description of stationary and time-resolved optical spectra of the CP43, CP47, and D1−D2−cyt$b$559 subunits and whole core complexes. It shows that the decay of excited states in PS-II core complexes with functional (open) reaction centers (RCs) is limited by the excitation energy transfer from the CP43 and CP47 core antennae to the RC occurring with a time constant of 40−50 ps at room temperature. The chlorophylls responsible for the low energy absorbance bands in the CP43 and CP47 subunits are assigned, and their signatures in hole burning, fluorescence line narrowing, and triplet-minus-singlet spectra are explained. The different locations of these trap states in the CP43 and CP47 antennae with respect to the reaction center lead to a dramatic change of the transfer dynamics at low temperatures. The calculations predict that, compared to room temperature, the fluorescence decay at 77 K should reveal a faster transfer from CP43 and a much slower and highly dispersive transfer from CP47 to the RC. A factor of 3 increase in the fastest decay time constant of fluorescence that was reported to occur when the RC is closed (the plastoquinone Q_A is reduced) is understood in the present model by assuming that the intrinsic rate constant for primary electron transfer decreases from 100 fs^{-1} for open RCs to 6 ps^{-1} for closed RCs, leading to a reduction of the primary electron acceptor Pheo$_{D1}$, in 300 fs and 18 ps, respectively. The model suggests that the reduced Q_A switches the photosystem into a photoprotective mode in which a large part of the excitation energy of the RC returns to the CP43 and CP47 core antennae, where the physiologically dangerous triplet energy of the chlorophylls can be quenched by the carotenoids. Experiments are suggested to test this hypothesis. The ultrafast primary electron transfer inferred for open RCs provides further support for the accessory chlorophyll Chl$_{D1}$ to be the primary electron donor in photosystem II.

Introduction

Photosynthesis provides the food and oxygen for our life. In plants and oxygenic photosynthetic bacteria, two photosystems working in series perform the transformation of solar energy into chemical energy. In both photosystem I[1] and photosystem II (PS-II),[2,3] a few reaction center pigments are surrounded by a large number of antennae pigments that collect the light and transfer the excitation energy via an exciton mechanism to the reaction center (RC). The excitation energy is used there to drive electron-transfer reactions. From the excited state P* of the RC an electron is transferred to the pheophytin of the electron transfer active D1 branch, Pheo$_{D1}$, and a charge-separated state, P$^+$ Pheo$_{D1}^-$, is formed. The electron is transferred further to the plastoquinone Q_A and the hole via a tyrosine, Tyr$_Z$, to the oxygen-evolving center (recent reviews are given in refs 4−7).

In the latter, water is used as an electron source and is split into molecular oxygen that we breath and protons that drive the synthesis of ATP.

As noted above, nature has functionalized the chlorophylls (Chls) in different ways. They act as light-harvesting pigments in the antennae and perform electron transfer in the RC. Besides the tuning of optical and electrochemical properties by the protein environment, the interpigment distances are important. A relatively large separation between the reaction center and the antenna pigments appears to be a general building principle for this type of complex. In this way oxidative/reductive side reactions involving the antenna pigments can be avoided. This aspect seems to be particularly important for photosystem II because of the high oxidative power of the reaction center Chls required for the water-splitting reaction.

Different Views about the Relative Time Scale of Exciton Transfer and Charge Separation. Despite a long history of experimental studies on the primary excitation energy and

(1) Jordan, P.; Fromme, P.; Witt, H. T.; Klukas, O.; Saenger, W.; Krauss, N. *Nature* **2001**, *411*, 909.
(2) Ferreira, K. N.; Iverson, T. M.; Maghlaouli, K.; Barber, J.; Iwata, S. *Science* **2004**, *303*, 1831.
(3) Loll, B.; Kern, J.; Saenger, W.; Zouni, A.; Biesiadka, J. *Nature* **2005**, *438*, 1040.
(4) Dekker, J; van Grondelle, R. *Photosynth. Res.* **2000**, *63*, 195.
(5) Diner, B. A.; Rappaport, F. *Annu. Rev. Plant Biol.* **2002**, *53*, 551.
(6) *Photosystem II: The Light-Driven Water Plastoquinone Oxidoreductase*; Wydrzynski, T., Satoh, K., Eds.; Springer: Dordrecht, The Netherlands, 2005.
(7) Kern, J.; Renger, G. *Photosynth. Res.* **2007**, *94*, 183.

charge-transfer reactions in PS-II, different views exist about the kinetic and mechanistic details. At the extreme there is the so-called excited-state radical pair equilibrium (ERPE) model[8−12] that assumes the equilibration of excited states in the whole core complex to be fast compared to the primary electron-transfer reaction in the RC. This trap-limited model was used to explain the variable fluorescence observed for open and closed reaction centers[8,9] and for PS-II complexes of different sizes.[10] Holzwarth and co-workers in early experiments observed[8,9] that the fastest component detected for the fluorescence decay of PS-II core complexes slows from 80 ps for open RCs to 220 ps for closed RCs, that is, by a factor of almost 3. The main 40 ps time constant observed in recent time-resolved fluorescence[11] and pump−probe spectra[12] on PS-II core complexes with open RCs was explained within the ERPE model by reversible electron transfer, assuming that the equilibration time of excited states in the whole system is about 1.5 ps and that primary charge separation, that is, the reduction of Pheo$_{D1}$, takes about 3 ps.

The ERPE model was challenged by studies on PS-II containing membranes (BBY particles)[13] and PS-II core complexes,[14,15] which reported evidence for relatively slow excitation energy transfer. From recent time-resolved visible pump/ mid-infrared probe studies[15] a 20−30 ps time constant for exciton relaxation between CP43, CP47, and the RC[15] was inferred. The same technique was applied to D1−D2−cyt$b$559 RC complexes, and it was concluded that the reduction of Pheo$_{D1}$ occurs in 600−800 fs.[16] In this case electron transfer in the RC is much faster than excitation energy transfer to the RC, and the decay of excited states is limited by the transfer to the trap. Alternative to this transfer-to-the-trap limited model, from time-resolved fluorescence data of RC−CP47 complexes it was concluded that the decay of excited states is neither trap nor transfer-to-the-trap limited, but that primary charge separation and excitation energy transfer occur on the same time scale.[17]

Objectives and Theoretical Aspects. A main goal of the present paper is to provide an answer to the following question: *What is the bottleneck for the decay of excited states in PS-II core complexes?* Besides the controversial interpretations of experimental studies discussed above, there have been calculations by Vasiliev and co-workers on this point.[18,19] The latter have led to the conclusion that the decay is limited by the transfer to the trap. However, localized excited states were assumed, and the site energies used in the calculations were assigned without calculations of optical spectra. In addition, the energy transfer calculations were based on a preliminary structural model[18] in which about 50% of the transition dipole moments were incorrectly assigned, with nearly perpendicular directions with respect to the true orientations that were resolved in the recent structural study.[3] All of these shortcomings have to be overcome to provide a definite answer to the above question. There are two main problems for the theory: (1) to take into account both the excitonic and the exciton−vibrational coupling in an appropriate way and (2) to assign realistic site energies to the 35 Chl a and 2 Pheo a molecules that are bound in the PS-II core complex. A site energy is defined as the hypothetical optical transition energy of a pigment in its binding site in the protein for absent excitonic coupling with the other pigments.

If one of the two types of couplings in problem 1 dominates, there are standard theories to describe the spectra and the excitation energy transfer. In the case of strong excitonic coupling, the excited states will be delocalized and the excitons will relax between these delocalized states, as described by Redfield theory (e.g., ref 20) or modified Redfield theory.[21−23] In the other limit, localized states are excited, and Förster theory[24,25] describes the transfer between these states. One aspect, often overlooked, is that the excited states are not only localized by static disorder but also by the dynamic modulation of transition energies. Even if two pigments have the same site energy, their excited states are delocalized only if the excitonic coupling is comparable to or larger than the nuclear reorganization energy of the local optical transitions. This aspect is particularly important if one of the two pigments represents a sink for the excitation energy, for example, because electron transfer starts from this pigment. Without dynamical localization, the excitation energy of the other pigment would be immediately quenched, independent of the strength of excitonic coupling between the two pigments, if they happen to have the same site energy. Dynamical localization, in the case of weak excitonic coupling, requires excitation energy transfer to the sink before the quenching.

Unfortunately, at present there exists no line shape theory that can describe lifetime broadening and vibrational sidebands[26] and, in addition, a dynamic localization of exciton states.[27] However, the latter may be treated implicitly by assuming that delocalized excited states can be formed only between pigments that are coupled more strongly than their local reorganization energy of the exciton−vibrational coupling.[28] If such domains are defined, exciton transfer between the domains is described by generalized Förster theory,[29−34] whereas the exciton relax-

(8) Schatz, G. H.; Brock, H.; Holzwarth, A. R. *Proc. Natl. Acad. Sci. U.S.A.* **1987**, *84*, 8414.

(9) Schatz, G. H.; Brock, H.; Holzwarth, A. R. *Biophys. J.* **1988**, *54*, 397.

(10) Barter, L. M. C.; Bianchietti, M.; Jeans, C.; Schilstra, M. J.; Hankamer, B.; Diner, B. A.; Barber, J.; Durrant, J. R.; Klug, D. R. *Biochemistry* **2001**, *40*, 4026.

(11) Miloslavina, Y.; Szczepaniak, M.; Müller, M. G.; Sander, J.; Nowaczyk, M.; Rögner, M.; Holzwarth, A. R. *Biochemistry* **2006**, *45*, 2436.

(12) Holzwarth, A. R.; Müller, M. G.; Reus, M.; Nowaczyk, M.; Sander, J.; Rögner, M. *Proc. Natl. Acad. Sci. U.S.A.* **2006**, *103*, 6895.

(13) Broess, K.; Trinkunas, G.; van der Wei-de Wit, C. D.; Dekker, J. P.; van Hoek, A.; van Amerongen, H. *Biophys. J.* **2006**, *91*, 3776.

(14) Jennings, R. G.; Elli, G.; Garlaschi, F. M.; Santabarbara, S.; Zucchelli, G. *Photosynth. Res.* **2000**, *66*, 225.

(15) Pawlowicz, N. P.; Groot, M.-L.; Van Stokkum, I. H. M.; Breton, J.; van Grondelle, R. *Biophys. J.* **2007**, *93*, 2732.

(16) Groot, M.-L.; Pawlowicz, N. P.; Van Wilderen, L. J. G. W.; Breton, J.; Van Stokkum, I. H. M.; van Grondelle, R. *Proc. Natl. Acad. Sci. U.S.A.* **2005**, *102*, 13087.

(17) Andrizhiyevskaya, E. G.; Frolov, D.; van Grondelle, R.; Dekker, J. P. *Phys. Chem. Chem. Phys.* **2004**, *6*, 4810.

(18) Vasilev, S.; Orth, P.; Zouni, A.; Owens, T. G.; Bruce, D. *Proc. Natl. Acad. Sci. U.S.A.* **2001**, *98*, 8602.

(19) Vasilev, S.; Lee, C. I.; Brudvig, G. W.; Bruce, D. *Biochemistry* **2002**, *41*, 12236.

(20) Renger, T.; May, V.; Kühn, O. *Phys. Rep.* **2001**, *343*, 138.

(21) Zhang, W. M.; Meier, T.; Chernyak, V.; Mukamel, S. *J. Chem. Phys.* **1998**, *108*, 7763.

(22) Yang, M.; Fleming, G. R. *Chem. Phys.* **2002**, *275*, 355.

(23) Renger, T.; Marcus, R. A. *J. Phys. Chem. A* **2003**, *107*, 8404.

(24) Förster, T. *Ann. Phys.* **1948**, *2*, 55.

(25) May, V.; Kühn, O. *Charge and Energy Transfer Dynamics in Molecular Systems: A Theoretical Introduction*; Wiley-VCH: Berlin, Germany, 2000.

(26) Renger, T.; Marcus, R. A. *J. Chem. Phys.* **2002**, *116*, 9997.

(27) Renger, T. *Phys. Rev. Lett.* **2004**, *93*, art. no. 188101.

(28) Yang, M.; Damjanovic, A.; Vaswani, H. M.; Fleming, G. R. *Biophys. J.* **2003**, *85*, 140.

(29) Fetisova, Z.; Freiberg, A.; Mauring, K.; Novoderezhkin, V.; Taisova, A.; Timpmann, K. *Biophys. J.* **1996**, *71*, 995.

(30) Sumi, H. *J. Phys. Chem. B* **1999**, *103*, 252.

(31) Mukai, K.; Abe, S.; Sumi, H. *J. Phys. Chem. B* **1999**, *103*, 6096.

(32) Scholes, G. D.; Fleming, G. R. *J. Phys. Chem. B* **2000**, *104*, 1854.

ation within the domains is treated by Redfield theory or modified Redfield theory.

Concerning point 2, an estimation of the site energies can be obtained from a fit of optical spectra of the subunits. The site energies of the RC pigments were previously determined and verified from a description of a large number of optical spectra of D1−D2−cyt$b$559 complexes.[35] The site energies determined for the RC pigments in D1−D2−cyt$b$559 preparations also describe optical difference spectra of the RC pigments in PS-II core preparations.[36] There are two minor differences: (i) The site energy of the accessory Chl of the D1 branch, Chl$_{D1}$, is red-shifted by 4 nm in PS-II core complexes and less inhomogeneously distributed. (ii) Besides the site energy of Chl$_{D1}$ that shows the same temperature dependence in core complexes as in D1−D2−cyt$b$559 complexes,[35] in core complexes also the site energy of P$_{D1}$ shifts with temperature, from 666 nm at 5 K to 670 nm at room temperature.[36] The site energies of the remaining pigments are temperature independent. In the present work, the site energies of the CP43 and CP47 subunits are determined from a fit of their experimental linear optical spectra[37−40] and verified by calculations of time-resolved pump−probe spectra and comparison with experimental data.[41]

Experimental Facts about Low-Energy Absorbance Bands in CP43 and CP47. Important information about the low-energy states, the so-called trap states in the CP43 and CP47 subunits, was obtained from spectroscopy in the frequency domain.[37−40,42−44] Excitation-dependent fluorescence line-narrowing spectra[37] gave first evidence that in CP43 at low temperatures there are two emitting states with different inhomogeneous distributions. From the vibrational fine structure of the excitation-dependent emission it was inferred that one of the two low-energy states is due to Chls with a hydrogen bond between their 13^1-keto group and the protein, whereas the other state showed signatures of six-coordinated Chls that do not form such hydrogen bonds. The Stark and triplet-minus-singlet (T−S) spectra provided evidence about partially delocalized excited states in CP43.[37]

The two quasi-degenerate low-energy states in CP43 were further characterized by non-photochemical hole burning (NPHB) and triplet bottleneck hole burning spectra by Jankowiak et al.,[43] who termed these states A- and B-states. Interestingly, the A-state was found to mainly contribute to the triplet bottleneck spectrum, whereas the B-state was detected, instead, in the NPHB spectrum.[43] These findings were explained by assuming a longer lifetime of the triplet state of A and that most of the

excitation energy from higher energy exciton states is trapped by the B-state.[43] Some evidence for excitonic coupling of the B-state pigments was reported from high-energy satellite holes at 673 and 678 nm.[43] Recently, Hughes et al.[44] investigated CP43 complexes with NPHB and non-wavelength-selective photoconversion spectroscopy. They proposed a different intrinsic photoconversion efficiency of the A- and B-states due to the strong hydrogen bond of the B-state Chls reported earlier by Groot et al.[37] This explanation allows both low-energy states to participate equally in excitation energy transfer to the RC, whereas Jankowiak et al.[43] inferred from the narrow zero−zero line widths in their NPHB data that the two states are uncoupled and therefore located in different layers in the membrane. From circular dichroism difference spectra, Hughes et al.[44] reported evidence that the B-state is excitonically correlated with higher energy states at 677 and 682 nm.

The low-energy states of CP47 were studied in great detail by de Weerd et al.[38] From a Gaussian band fitting of the absorption and linear dichroism spectra, it was concluded that the low-energy state around 690 nm is due to a monomeric Chl with a distinct orientation of its Qy-transition relative to the membrane plane (with an angle larger than 35°) and that the next higher excited state around 683 nm carries the oscillator strength of approximately three Chls. The finding about the 690 nm emitting Chl supported earlier investigations of van Dorson et al.[42] From polarized emission measurements, de Weerd et al.[38] obtained additional evidence for a single emitting state at 690 nm. The depolarized 683 nm emission was interpreted by assuming that at least two isoenergetic states with nonparallel transition dipole moments contribute. From the vibrational fine structure in the FLN spectra it was inferred that there is a strong hydrogen bond between the 13^1-keto group of the 690 nm monomeric Chl and the protein, whereas the Chls contributing to the 683 nm states form less strong hydrogen bonds.[38] Additional evidence for the monomeric nature of the 690 nm state was reported from the relative decrease of a 80 cm^{-1} mode at long wavelengths in the emission. This mode is thought to represent intermolecular vibrations modulating the coupling between pigments.[45] Interestingly, the T−S spectra did show no bleaching at 690 nm, but only the 683 nm state appeared along with some higher energy satellites that were taken as evidence for the delocalized nature of the 683 nm state.[38] Two alternatives were offered for the absence of a 690 nm bleaching in the T−S spectra: either an artifact due to the high excitation power leading to a permanent bleaching of this state or an efficient quenching of the triplet state formed at the 690 nm Chl by a nearby carotenoid.[38]

The fluorescence of the 690 nm state that gives rise to an emission maximum at 695 nm was used as a marker for the presence of PS-II core complexes in thylakoid membranes in mutation experiments on various histidines in CP47 by Shen and Vermaas.[46] When His B114 was mutated to Tyr, the 695 nm band was completely lost and also no O$_2$ evolution was detectable, whereas a mutation of His B114 to Gln led to a 70% reduction in the amplitude of the 695 nm emission and O$_2$ evolution and in addition to a blue shift of the emission to 693

(33) Jang, S.; Newton, M. D.; Silbey, R. J. *Phys. Rev. Lett.* **2004**, *92*, art. no. 218301.
(34) Müh, F.; Madjet, M. E.; Adolphs, J.; Abdurahman, A.; Rabenstein, B.; Ishikita, H.; Knapp, E. W.; Renger, T. *Proc. Natl. Acad. Sci. U.S.A.* **2007**, *104*, 16862.
(35) Raszewski, G.; Saenger, W.; Renger, T. *Biophys. J.* **2005**, *88*, 986.
(36) Raszewski, G.; Diner, B. A.; Schlodder, E.; Renger, T. *Biophys. J.*, in press.
(37) Groot, M. L.; Frese, R. N.; de Weerd, F. L.; Bromek, K.; Petterson, Å.; Peterman, E. J. G.; van Stokkum, I. H. M.; van Grondelle, R.; Dekker, J. P. *Biophys. J.* **1999**, *77*, 3328.
(38) de Weerd, F. L.; Palacios, M. A.; Andrizhiyevskaya, E. G.; Dekker, J. P.; van Grondelle, R. *Biochemistry* **2002**, *41*, 15224.
(39) Groot, M. L.; Peterman, E. J. G.; van Stokkum, I. H. M.; Dekker, J. P.; van Grondelle, R. *Biophys. J.* **1995**, *68*, 281.
(40) Alfonso, M.; Montoya, G.; Cases, R.; Rodriguez, R.; Picorel, R. *Biochemistry* **1994**, *33*, 10494.
(41) de Weerd, F. L.; van Stokkum, I. H. M.; van Amerongen, H.; Dekker, J. P.; van Grondelle, R. *Biophys. J.* **2002**, *82*, 1586.
(42) Van, Dorsson, R. J.; Plijter, J. J.; Dekker, J. P.; Den, Ouden, A.; Amesz, J. *Biochim. Biophys. Acta* **1987**, *890*, 134.
(43) Jankowiak, R.; Zazubovich, V.; Rätsep, M.; Matsuzaki, S.; Alfonso, M.; Picorel, R.; Seibert, M.; Small, G. J. *J. Phys. Chem. B* **2000**, *104*, 11805.
(44) Hughes, J. L.; Picorel, R.; Seibert, M.; Krausz, E. *Biochemistry* **2006**, *45*, 12345.

(45) Peterman, E. J. G.; van Amerongen, H.; van Grondelle, R.; Dekker, J. P. *Proc. Natl. Acad. Sci. U.S.A.* **1998**, *95*, 6128.
(46) Shen, G.; Vermaas, W. F. J. *Biochemistry* **1994**, *33*, 7379.

nm. These results were taken as evidence that His B114 and the Chl it binds are important for the assembly and function of PS-II.[46]

In the present study we will suggest the molecular identities of the above trap states in CP43 and CP47 and explain their signatures in the various spectra.

Time-Resolved Experiments on Exciton Transfer in CP43 and CP47. The excitation energy transfer in CP43 and CP47 was investigated by time-resolved absorption and fluorescence spectroscopy[41] at 77 K. In both complexes, time constants of 0.2–0.4 and 2–3 ps were found that were attributed to exciton transfer between Chls in the same, stromal or lumenal, layer and that between pigments in different layers, respectively. In CP47, in addition, a slower 17–28 ps component was detected for transfer to the 690 nm trap state. The present calculations provide a structure-based analysis of these pump–probe spectra and also serve to check the exciton relaxation times predicted by the theory. It is important to note that no adjustable parameter is used to tune the transfer rates. This approach was successfully tested in calculations of exciton relaxation in smaller complexes before.[34,35,47–49]

Theory

In the following, we briefly summarize the theory of optical spectra and excitation energy transfer and the parameters entering the theory.

Hamiltonian. The Chls of the pigment–protein complex (PPC) are described as two-level systems including their ground (S_0) and excited (S_1) state. The Hamiltonian of the PPC contains four parts:

$$H = H_{ex} + H_{ex-vib} + H_{vib} + H_{ex-rad} \quad (1)$$

The excitonic part H_{ex} contains the energies of the localized one- and two-exciton states $|m>$ and $|mn>$, respectively, and the excitonic couplings $V_{10,01}$ between different one- and two-exciton states:

$$H_{ex} = E_m|m><m| + \sum_{m>n}(E_m + E_n + \delta_{mn}^{(2exc)})|mn><mn| + \sum_{m,n} V_{10,01}(m,n)|m><n| + \sum_{m>n}\sum_k V_{10,01}(m,k)|mn><kn| \quad (2)$$

In $|m>$, the mth pigment is excited and all others are in the ground S_0 state, whereas in $|mn>$, in addition to the mth pigment, the nth pigment is excited. The excitonic coupling $V_{10,01}(m,n)$ describes the Coulomb interaction between the transition densities of the ground-to-excited state transitions of pigments m and n. Any double excitation of a single pigment[50] is neglected, for simplicity. The energies of the two-exciton states in eq 2 contain the two-exciton shift $\delta_{mn}^{(2exc)}$

$$\delta_{mn}^{(2exc)} = V_{11,11}(m,n) - V_{11,00}(m,n) - V_{00,11}(m,n) \quad (3)$$

that results from the charge density coupling $V_{aa,bb}(m,n)$ between the state m of pigment a and the state n of pigment b, as derived in the Supporting Information (SI). The two-exciton shifts $\delta_{mn}^{(2exc)}$, which are usually neglected, are included in the present treatment because they have an influence on the nonlinear spectra. The charge density couplings $V_{aa,bb}(m,n)$ as well as the excitonic couplings $V_{10,01}(m,n)$ are obtained by a method developed previously[51] (see below).

(47) Renger, T.; Marcus, R. A. *J. Phys. Chem. B* **2002**, *106*, 1809.
(48) Adolphs, J.; Renger, T. *Biophys. J.* **2006**, *91*, 2778.
(49) Renger, T.; Trostmann, I.; Theiss, C.; Madjet, M. E.; Richter, M.; Paulsen, H.; Eichler, H. J.; Knorr, A.; Renger, G. *J. Phys. Chem. B* **2007**, *111*, 10487.
(50) Renger, T.; May, V. *Photochem. Photobiol.* **1997**, *66*, 618.
(51) Madjet, M. E.; Abdurahman, A.; Renger, T. *J. Phys. Chem. B* **2006**, *110*, 17268.

The modulation of pigment transition energies by the protein dynamics, contained in H_{ex-vib}, is described by the spectral density $J(\omega)$.[26] The vibrations are treated as harmonic oscillators in H_{vib}, and the coupling to external light fields is described by H_{ex-rad} in rotating wave approximation. Explicit forms for H_{ex-vib}, H_{vib}, and H_{ex-rad} are given in ref 26.

(a) Domains of Strongly Coupled Pigments. If the excitonic coupling between the optical transitions of the pigments is larger than the static and dynamic disorder by the pigment–protein coupling, a delocalized excited state is formed. The localization of exciton states by static disorder in site energies is included in the calculations by a Monte Carlo method used to generate the disorder and to average the spectra obtained for the different sets of site energies. Dynamic localization is modeled implicitly by allowing delocalization only between those pigments, for which the excitonic coupling is comparable to or stronger than the local dynamic disorder. A quantitative measure of the latter is the reorganization energy of the optical transition

$$E_\lambda = \int d\omega \hbar\omega J(\omega) \quad (4)$$

that describes the energy that is released when the nuclei relax to a new equilibrium position after optical excitation of a pigment. If two pigments m and n are coupled by an excitonic coupling $V_{10,01}(m,n)$ that is comparable to or larger than the reorganization energy E_λ, they are included in the same domain d. One-exciton states

$$|M_d> = \sum_{m_d} c_{m_d}^{(M_d)}|m_d> \quad (5)$$

and two-exciton states

$$|2M_d> = \sum_{m_d>n_d} c_{m_d n_d}^{(2M_d)}|m_d n_d> \quad (6)$$

are obtained for the pigments in one domain by diagonalization of the exciton Hamiltonian that contains in the diagonal the site energies and in the off-diagonal the excitonic couplings. After this diagonalization, the exciton Hamiltonian H_{ex} in eq 2 becomes

$$H_{ex} = \sum_d \sum_{M_d} \epsilon_{M_d}|M_d><M_d| + \sum_{2M_d} \epsilon_{2M_d}|2M_d><2M_d| + \sum_{a\neq b}\sum_{M_a,N_b} V_{M_a N_b}|M_a><N_b| \quad (7)$$

with the energies of the delocalized one- and two-exciton states ϵ_{M_d} and ϵ_{2M_d}, respectively, and the coupling $V_{M_a N_b}$ between delocalized one-exciton states $|M_a>$ and $|N_b>$ in different domains a and b, respectively

$$V_{M_a N_b} = \sum_{m_a,n_b} c_{m_a}^{(M_a)} c_{n_b}^{(N_b)} V_{10,01}(m_a,n_b) \quad (8)$$

where $V_{10,01}(m_a,n_b)$ is the excitonic coupling between the optical transitions of pigment m_a in domain a and n_b in b. We note that in the present limit of low pump intensities a population of two-exciton states can be neglected. Therefore, it is not necessary to take into account the coupling between two-exciton states in different domains.

Linear Optical Spectra. The linear optical spectra are obtained as a sum over the domain spectra. The absorption spectrum $\alpha(\omega)$ follows as

$$\alpha(\omega) = \sum_d \alpha_d(\omega) = \sum_d \langle \alpha_d^{(hom)}(\omega)\rangle_{dis} \quad (9)$$

where $\langle...\rangle_{dis}$ denotes an average over the disorder in site energies. An independent variation of the site energies is assumed described by a Gaussian distribution function of the same width Δ_{inh} for all sites, with

one exception. The inhomogeneous distribution of the site energy of Chl_{D1} is chosen to be 40% smaller. This result was obtained on the basis of calculations of optical difference spectra of the RC pigments and comparison with experimental data, in particular, the triplet-minus-singlet spectrum.[36] The disorder average is performed numerically by a Monte Carlo method.

The homogeneous absorption of domain d is obtained as

$$\alpha_d^{(hom)}(\omega) \propto \omega \sum_{M_d} |\mu_{M_d}|^2 D_{M_d}(\omega) \qquad (10)$$

with the transition dipole moment

$$\vec{\mu}_{M_d} = \sum_{m_d} c_{m_d}^{(M_d)} \vec{\mu}_{m_d} \qquad (11)$$

where $\vec{\mu}_{m_d}$ is the local transition dipole moment of pigment m_d. The line shape function $D_{M_d}(\omega)$ was obtained from a non-Markovian POP-line shape theory within secular approximation and Markov approximation for the off-diagonal elements of the exciton–vibrational coupling:[26]

$$D_{M_d}(\omega) = \frac{1}{2\pi} \int_{-\infty}^{\infty} dt e^{i(\omega-\tilde{\omega}_{M_d0})t} \, e^{G_{M_d}(t)-G_{M_d}(0)} e^{-|t|/\tau_{M_d}} \qquad (12)$$

The time-dependent function $G_{M_d}(t)$ describes the vibrational sideband of the exciton transition, the dephasing time τ_{M_d} describes the lifetime broadening due to exciton relaxation, and $\tilde{\omega}_{M_d0}$ is the transition frequency that is shifted from the exciton transition frequency $\omega_{M_d0} = \epsilon_{m_d}/\hbar$ by the exciton–vibrational coupling.[26,52] All of these quantities depend on the exciton coefficients $c_m^{(M)}$, the spectral density $J(\omega)$, the correlation radius of protein vibrations R_c,[20,26,53] and the mean number of vibrational quanta $n(\omega)$ that are excited at a given temperature (Bose–Einstein distribution function). Explicit expressions for these quantities are given in the SI.

In the calculation of the linear dichroism (LD) and circular dichroism (CD) spectra the same disorder average as for linear absorption and the same line shape function $D_{M_d}(\omega)$ in eq 12 are used, but the $|\mu_{M_d}|^2$ in eq 10 is replaced in the calculation of CD by the rotational strength

$$r_{M_d} = \sum_{m_d > n_d} c_{m_d}^{(M_d)} c_{n_d}^{(M_d)} \vec{R}_{m_d n_d} \cdot \vec{\mu}_{m_d} \times \vec{\mu}_{n_d} \qquad (13)$$

and in the case of LD by

$$|\mu_{M_d}|^2 (1 - 3\cos^2(\theta_{M_d})) \qquad (14)$$

Here, θ_{M_d} is the angle between the transition dipole moment $\vec{\mu}_{M_d}$ and the membrane normal, and the vector $\vec{R}_{m_d n_d} = \vec{R}_{n_d} - \vec{R}_{m_d}$ in eq 13 connects the centers of pigments m_d and n_d.

Emission starts from an excited state that is assumed to be relaxed in the potential energy surfaces of the exciton states.[26] The resulting homogeneous fluorescence signal $I_d^{(hom)}(\omega)$ reads[26]

$$I_d^{(hom)}(\omega) \propto \omega^3 \sum_{M_d} f(M_d) |\mu_{M_d}|^2 D'_{M_d}(\omega) \qquad (15)$$

with the Boltzmann factor

$$f(M_d) = e^{-\epsilon_{M_d}/kT} / \sum_{N_d} e^{-\epsilon_{N_d}/kT} \qquad (16)$$

and the emission line shape function

(52) Renger, T.; May, V. *Phys. Rev. Lett.* **2000**, *84*, 5228.
(53) Renger, T.; May, V. *J. Phys. Chem. A* **1998**, *102*, 4381.

$$D'_{M_d}(\omega) = \frac{1}{2\pi} \int_{-\infty}^{\infty} dt e^{-i(\omega-\tilde{\omega}_{M_d0})t} \, e^{G_{M_d}(t)-G_{M_d}(0)} e^{-|t|/\tau_{M_d}} \qquad (17)$$

which is a slightly simplified expression of our earlier result.[26]

Excitation by an Ultrashort Pump Pulse. The creation of exciton population by an ultrashort pump pulse is described in second-order perturbation theory in the exciton–radiational coupling and within rotating wave approximation. A Gaussian-shaped pulse envelope

$$E_\Omega(t) = \frac{E_0}{\sqrt{2\pi}\tau_p} e^{-t^2/(2\tau_p^2)} \qquad (18)$$

is assumed, where the full width at half-maximum (fwhm) of $E_\Omega(t)$ is $2\tau_p\sqrt{2\ln 2}$. Neglecting exciton relaxation, that is, the off-diagonal part of the exciton–vibrational coupling, during the action of the short pump pulse, the exciton population $P_{M_d}^{(d)}(0)$ created by such a pulse is obtained as[48]

$$P_{M_d}^{(d)}(0) =$$
$$\frac{E_0^2 |\vec{\mu}_{M_d}|^2}{6\hbar^2 \sqrt{\pi}\tau_p} \int_{-\infty}^{\infty} d\tau e^{-i(\Omega-\omega'_{M_d0})\tau} e^{G_{M_d}(\tau)-G_{M_d}(0)} e^{-\tau^2/(4\tau_p^2)} \qquad (19)$$

where $\omega'_{M_d0} = \omega_{M_d0} - \gamma_{M_d M_d} E_\lambda/\hbar$ with the E_λ in eq 4 and the $\gamma_{M_d M_d}$ in the SI, is the energy difference between the minima of the PES of exciton state $|M_d\rangle$ and the ground state $|0\rangle$ and Ω is the center frequency of the optical pulse. Equation 19 includes the diagonal part of the exciton–vibrational coupling, that is, the mutual shift of exciton potential energy surfaces, without approximation.

Excitation Energy Transfer. (a) Intradomain Exciton Relaxation. Exciton relaxation between different exciton states $|M_d\rangle$ and $|N_d\rangle$ in the same domain d is described by the Redfield rate constant (e.g., ref 20)

$$k_{M_d \to N_d} = 2\pi \gamma_{M_d N_d} \omega_{M_d N_d}^2 \times$$
$$\{J(\omega_{M_d N_d})(1 + n(\omega_{M_d N_d})) + J(\omega_{N_d M_d}) n(\omega_{N_d M_d})\} \qquad (20)$$

where $\gamma_{M_d N_d}$ depends on the exciton coefficients and the correlation radius of protein vibrations (see SI).

(b) Interdomain Exciton Transfer. Exciton transfer between excited states in different domains a and b is described by the rate constant $k_{M_a \to N_b}$ obtained using generalized Förster theory as[29−34]

$$k_{M_a \to N_b} = 2\pi \frac{|V_{M_a N_b}|^2}{\hbar^2} \int_{-\infty}^{\infty} d\omega D'_{M_a}(\omega) D_{N_b}(\omega) \qquad (21)$$

with the interdomain exciton coupling $V_{M_a N_b}$ in eq 8. The functions $D'_{M_a}(\omega)$ and $D_{N_b}(\omega)$ are the normalized fluorescence and absorption line shape functions of exciton states $|M_a\rangle$ and $|N_b\rangle$, respectively. The POP line shape functions in eqs 12 and 17 are used.

(c) Master Equation. The populations of exciton states are related by the following master equations

$$\frac{d}{dt} P_{M_a}^{(a)}(t) = -\sum_{d,N_d} (k_{M_a \to N_d} P_{M_a}^{(a)}(t) - k_{N_d \to M_a} P_{N_d}^{(d)}(t))$$

$$a = 1 \dots N_{dom}, \, M_a = 1 \dots N_{pig}^{(a)} \qquad (22)$$

where N_{dom} is the number of domains and $N_{pig}^{(a)}$ is the number of pigments in domain a. For the rate constants $k_{M_a \to N_d}$, the Redfield expression in eq 20 is used, if $a = d$, and the generalized Förster rate constant in eq 21 is used if $a \neq d$. In matrix form eq 22 reads $(d/dt)\vec{P}(t) = -A\vec{P}(t)$, where the exciton populations are the elements of $\vec{P}(t)$ and the kinetic matrix A contains in the diagonal the elements $A_{M_a M_a} =$

$\sum_{d,N_d} k_{M_a \to N_d}$ and in the off-diagonal $A_{M_a N_d} = -k_{N_d \to M_a}$. The standard solution for $\vec{P}(t)$ is given as

$$\vec{P}(t) = \sum_i d_i \vec{c}_i e^{-\lambda_i t} \tag{23}$$

where the λ_i and $\vec{c}_i$ are the eigenvalues and (right) eigenvectors of the kinetic matrix A, respectively. The constants d_i are obtained from the initial condition $\vec{P}(0) = \sum_i d_i \vec{c}_i$, where the element $P_{M_a}^{(a)}(0)$ of $\vec{P}(0)$ is the initial population of the exciton state $|M_a>$ in domain a created by the short pulse (eq 19). In the case of PS-II core complexes, in addition to the exciton states, radical pair states are included that are coupled to the exciton states as described further below.

Time-Resolved Pump–Probe Spectra. In pump–probe spectroscopy, the pigment–protein complex is excited by a short pump pulse and the excitation energy transfer/relaxation is tested by a delayed probe pulse. It is assumed that the delay τ_d between the probe pulse and the pump pulse is large enough so that any vibrational coherences or coherences between different exciton levels have decayed when the probe–pulse interacts with the complex. A delta function-shaped probe pulse $E_0^{(pr)} \vec{e}_{pr} \delta(\tau_d)$ is used with polarization vector $\vec{e}_{pr}$. This delta pulse is an idealization of a short experimental probe pulse with a white spectrum. The pump–probe signal $\Delta\alpha(\tau_d)$ is the difference between the absorption measured by the probe pulse at a delay time τ_d after the pump pulse and the absorption measured by the probe pulse alone. If the probe pulse is dispersed in a monochromator after the sample, in addition to the dependence on the delay time, also the frequency dependence of $\Delta\alpha(\tau_d) = \int d\omega \Delta\alpha_{disp}(\tau_d, \omega)$ can be measured. The dispersed pump–probe signal $\Delta\alpha_{disp}(\tau_d, \omega)$, in the present approximation, has three contributions

$$\Delta\alpha_{disp}(\tau_d, \omega) \propto GB(\omega) + SE(\omega, \tau_d) + ESA(\omega, \tau_d) \tag{24}$$

time-independent ground-state bleaching $GB(\omega)$, time-dependent stimulated emission $SE(\omega, \tau_d)$, and time-dependent excited-state absorption $ESA(\omega, \tau_d)$. Using a POP-line shape theory, the following expressions are obtained[26]

$$GB(\omega) = -\left\langle \sum_d \sum_{M_d} (\mu_{M_d}^{(pr)})^2 D_{M_d}(\omega) \sum_{K_d} P_{K_d}^{(d)}(0) \right\rangle_{(dis+orient)} \tag{25}$$

with $\mu_{M_d}^{(pr)} = \vec{\mu}_{M_d} \vec{e}_{pr}$, the $P_{K_d}^{(d)}(0)$ in eq 19, and the absorption line shape function $D_{M_d}(\omega)$ in eq 12

$$SE(\omega) = -\left\langle \sum_d \sum_{M_d} (\mu_{M_d}^{(pr)})^2 D'_{M_d}(\omega) P_{M_d}(\tau_d) \right\rangle_{(dis+orient)} \tag{26}$$

with the fluorescence line shape function $D'_{M_d}(\omega)$ in eq 17 and the time-dependent exciton populations $P_{M_d}(\tau_d)$ obtained from the solution of the master equation (eq 22), and

$$ESA(\omega) = -\left\langle \sum_d \sum_{M_d, 2N_d} (\mu_{M_d \to 2N_d}^{(pr)})^2 D'_{M_d \to 2N_d}(\omega) P_{M_d}(\tau_d) \right\rangle_{(dis+orient)} \tag{27}$$

where $\mu_{M_d \to 2N_d}^{(pr)}$ is the scalar product between the probe pulse polarization vector $\vec{e}_{pr}$ and the transition dipole moment $\vec{\mu}_{M_d \to 2N_d}$ between the one-exciton state $|M_d>$ and the two-exciton state $|2N_d>$. The ESA line shape function $D'_{M_d \to 2N_d}(\omega)$ is given in the SI.

The $\langle ... \rangle_{dis+orient}$ in eqs 25–27 denotes an average over disorder in site energies and over the orientation of the complex with respect to the external pump and probe field polarizations. As in the experiments,[41] a magic angle (54.7°) is assumed between the polarizations of the pump and probe pulses, $\vec{e}_{pu}$ and $\vec{e}_{pr}$, respectively.

(a) Lifetime Density Map of Time-Dependent Emission. To illustrate the time and frequency dependence of exciton relaxation, lifetime density (LFD) maps of the time-dependent emission are

calculated. The time-dependent emission $I(\omega, t)$ is obtained as

$$I(\omega, t) \propto \omega^3 \left\langle \sum_{d,M_d} |\mu_{M_d}|^2 D'_{M_d}(\omega) P_{M_d}^{(d)}(t) \right\rangle_{(dis+orient)} \tag{28}$$

with the fluorescence line shape function $D'_{M_d}(\omega)$ in eq 17 and the exciton-state population $P_{M_d}^{(d)}(t)$, resulting from the solution of eq 22. Inspired by the Müller–Holzwarth LFD maps (e.g., ref 54), the emission $I(\omega, t)$ is expressed as

$$I(\omega, t) = \omega^3 \int_0^\infty d\tau \, A(\omega, \tau) e^{-t/\tau} \tag{29}$$

where $A(\omega, \tau)$ is the LFD map. By introducing eq 23 into eq 28 and comparison with eq 29 the LFD map $A(\omega, \tau)$ is obtained as

$$A(\omega, \tau) = \left\langle \sum_i \sum_{d,M_d} |\mu_{M_d}|^2 D'_{M_d}(\omega) d_i c_i^{(d,M_d)} \delta(\tau - \lambda_i^{-1}) \right\rangle_{(dis+orient)} \tag{30}$$

where $c_i^{(d,M_d)}$ is the component of exciton state M_d (in domain d) in the eigenvector $\vec{c}$ in eq 23. We note that the present calculation of the LFD map avoids an inverse Laplace transform that is needed if the map is obtained directly from experimental data.

Electron Transfer in the RC. Primary electron transfer in the RC is included phenomenologically by including three radical pair states RP1, RP2, and RP3 and assigning respective forward and backward rate constants for electron transfer. The following molecular identities are assumed for these states:[12,16,35] RP1 = Chl_{D1}^+ $Pheo_{D1}^-$, RP2 = P_{D1}^+ $Pheo_{D1}^-$, and RP3 = P_{D1}^+ Q_A^-, where P_{D1} is the "special pair" Chl of the D1-branch. The first radical pair state RP1 is created by electron transfer from the exciton states $|M>$ of the RC pigments with a rate constant

$$k_{M \to RP1} = |c_{Chl_{D1}}^{(M)}|^2 k_{intr} \tag{31}$$

where $|c_{Chl_{D1}}^{(M)}|^2$ is the probability of finding the primary electron donor Chl_{D1} excited in the exciton state $|M>$ and k_{intr} is the intrinsic rate constant for the reaction

$$Chl_{D1}^* \, Pheo_{D1} \xrightarrow{k_{intr}} Chl_{D1}^+ \, Pheo_{D1}^- \tag{32}$$
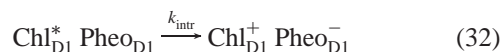
The forward and back reactions are approximately related by $k_{M \to RP1}/k_{RP1 \to M} \approx \exp\{\Delta G_{intr}^{(0)}/kT\}$, where $\Delta G_{intr}^{(0)}$ equals the difference in standard free energy of the intrinsic electron-transfer reaction in eq 32. The rate constants $k_{RP1 \to RP2}$ and $k_{RP2 \to RP1}$ are related by $k_{RP1 \to RP2}/k_{RP2 \to RP1} = \exp\{\Delta G_{RP1/RP2}/kT\}$. The free energy difference between RP2 and RP3 is assumed to be so large that a back reaction RP3 → RP2 can be neglected; that is, irreversible trapping at RP3 is assumed. For closed RCs (reduced Q_A) a double reduction of Q_A can be neglected on the relevant time scale considered here; that is, $k_{RP2 \to RP3} = 0$ in this case.

Compartment Models. (a) Fast Relaxation in Domains. If fast intradomain exciton relaxation is assumed, the exciton transfer between two domains starts from a (quasi) equilibrated excited-state manifold of the donor domain, and the interdomain transfer rate constant $k_{a \to b}$ becomes

$$k_{a \to b} = \sum_{M_a, N_b} f(M_a) k_{M_a \to N_b} \tag{33}$$

with the rate constant $k_{M_a \to N_b}$ in eq 21 and the Boltzmann factor $f(M_a)$ in eq 16. The primary electron-transfer rate constant in this limit is given as

(54) Müller, M. G.; Niklas, J.; Lubitz, W.; Holzwarth, A. R. *Biophys. J* **2003**, *85*, 3899.

$$k_{RC \to RP1} = \sum_{M_a}^{a=RC} f(M_a)|c_{Chl_{D1}}^{(M_a)}|^2 k_{intr} \quad (34)$$

where M_a counts the exciton states of the domain of the primary electron donor. This domain is formed by the six strongly coupled RC pigments.

(b) Fast Relaxation in Larger Compartments. For further simplification, different domains are included in a compartment I and fast equilibration of excitation energy is assumed in the whole compartment. The rate constant for excitation energy transfer between compartments I and J is then obtained as

$$k_{I \to J} = \sum_{a,b}^{a \epsilon I, b \epsilon J} \sum_{M_a, N_b} f(I, M_a) k_{M_a \to N_b} \quad (35)$$

where a and b count the domains in compartments I and J and $f(I, M_a)$ is the Boltzmann factor

$$f(I, M_a) = e^{-\epsilon_{Ma}/kT} / \sum_{c, K_c}^{c \epsilon I} e^{-\epsilon_{Kc}/kT} \quad (36)$$

The primary electron transfer between compartment I that contains the RC and RP1 is then obtained as

$$k_{I \to RP1}^{(RC \epsilon I)} = \sum_{M_a}^{a=RC} f(I, M_a)|c_{Chl_{D1}}^{(M_a)}|^2 k_{intr} \quad (37)$$

Compartments of different sizes are used below to find the bottleneck for the decay of excited states in PS-II core complexes.

Parameters. The parameters of the theory are (i) the excitonic and charge density couplings between the pigments, (ii) the spectral density of the pigment—protein coupling, and (iii) the site energies of the pigments. The excitonic couplings $V_{10,01}$ are obtained by the TrEsp method[51] as

$$V_{10,01}(m, n) = \sum_{I,J} \frac{q_I(1, 0)q_J(1, 0)}{|\mathbf{R}_I^{(m)} - \mathbf{R}_J^{(n)}|} \quad (38)$$

where I and J count the nuclei of pigments m and n, respectively, and $\mathbf{R}_I^{(m)}$ and $\mathbf{R}_J^{(n)}$ are the respective nuclear coordinates, at which the transition charges $q_I(1,0)$ and $q_J(1,0)$ are placed. The transition charges $q_I(1,0)$ of the $S_0 \to S_1$ transition were determined such as to fit the electrostatic potential of the transition density obtained with TDDFT using a B3LYP exchange correlation functional and a 6-31G* basis set, as explained in detail in ref 51. The charges were rescaled to yield an effective dipole moment of 4.4 D for Chl*a* and 3.5 D for Pheo that takes into account screening and local field effects of the Coulomb coupling in the dielectric of the protein in an effective way (more details and values for the excitonic couplings are given in the SI).

The charge density couplings $V_{aa,bb}$ in eq 3

$$V_{aa,bb}(m, n) = \frac{1}{\epsilon_{eff}} \sum_{I,J} \frac{q_I(a, a)q_J(b, b)}{|\mathbf{R}_I^{(m)} - \mathbf{R}_J^{(n)}|} \quad (39)$$

are calculated with the ground- and excited-state partial charges $q_I(0, 0)$ and $q_I(1,1)$ respectively. These charges were obtained from a fit of the electrostatic potential of the ground- and excited-state charge densities, respectively, using the same ab initio method as for the transition density. The ϵ_{eff} in eq 39 describes screening and local field effects that are due to the polarizability of the protein. At a temperature of 77 K of the pump—probe experiments,[41] $\epsilon_{eff} = 3$ is used, as determined from the calculations of absorbance difference of spectra of PS-II core complexes with oxidized and reduced reaction center

pigments.[36] In the calculation of excitonic couplings in eq 38 no such ϵ_{eff} appears, because the quantum chemical transition charges are rescaled to take into account these effects, whereas unscaled charges are used in eq 39. Please note also that in the case of the excitonic coupling just the electronic polarization of the protein is involved, whereas the charge density coupling is influenced, in addition, by the nuclear part of the polarization (which gives rise to a temperature dependence of ϵ_{eff}[36]).

The spectral density of the pigment—protein coupling in the B777 complex, consisting of a single bacteriochlorophyll *a* molecule coupled to an α-helix, was extracted recently[26] from fluorescence line-narrowing spectra measured[55] at 1.7 K. Here, the same normalized functional form $J_0(\omega)$ is assumed ($\int_0^\infty J_0(\omega) \, d\omega = 1$)

$$J_0(\omega) = \frac{1}{s_1 + s_2} \sum_{i=1,2} \frac{s_i}{7!2\omega_i^4} \omega^3 \, e^{-(\omega/\omega_i)^{1/2}} \quad (40)$$

with the extracted parameters $s_1 = 0.8$, $s_2 = 0.5$, $\hbar\omega_1 = 0.069$ meV, and $\hbar\omega_2 = 0.24$ meV. The spectral density $J(\omega)$ is described by[34,35,48,49]

$$J(\omega) = SJ_0(\omega) \quad (41)$$

A Huang—Rhys factor $S = 0.65$ is used for the RC pigments, which was estimated from the temperature dependence of the absorption spectrum of D1—D2—cyt*b*559 complexes.[35] The Huang—Rhys factor of the pigments in the core antenna subunits will be estimated from the temperature dependence of the absorption spectrum of CP43 complexes. The determination of S from the linear spectra allows one to describe the rate constants for exciton relaxation/transfer practically without free parameter.

The site energies of the pigments in the CP43 and CP47 core antennae are determined from a fit of linear absorption, linear dichroism, circular dichroism, and fluorescence spectra. In the case of CP47, these four spectra are used in the fit. For CP43, the circular dichroism spectrum is excluded, because the experimental spectrum is nonconservative and therefore cannot be described by the present exciton theory.

The rate constants for excitation energy transfer are determined by the site energies, the excitonic couplings, the spectral density and the correlation radius of protein vibrations R_c. For the latter a value of 5 Å is assumed, as determined from calculation of transient absorption spectra and comparison with experimental data on D1—D2—cyt*b*559 complexes[47] and on complexes of the water-soluble chlorophyll-binding protein (WSCP).[49]

Results

The Results section is organized in the following way. The calculations of stationary spectra of the CP43 and CP47 subunits and comparison with experimental data are used to determine the site energies of the pigments in these subunits and the Huang—Rhys factor of the exciton—vibrational coupling. The Huang—Rhys factor and the site energies are tested afterward in the calculation of time-resolved optical spectra and comparison with experimental data of the CP43 and CP47 complexes. Next, the parameters are used in calculations of the fluorescence decay of PS-II core complexes where the intrinsic rate constant of primary charge transfer is determined on the basis of a comparison of the calculations with the experimental fluorescence decay data. To find the bottleneck of the excited-state decay, various compartment models are studied by assuming fast equilibration of excited states in these compartments. Finally, calculations are performed for PS-II core complexes with closed RCs to explain the variable fluorescence.

(55) Creemers, T. M. H.; De Caro, C. A.; Visschers, R. W.; van Grondelle, R.; Völker, S. *J. Phys. Chem. B* **1999**, *103*, 9770.
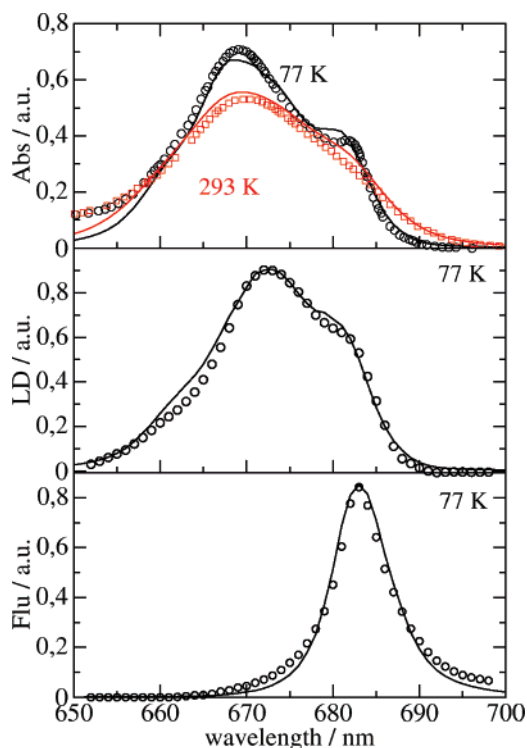
Figure 1. Absorption (Abs), linear dichroism (LD), and fluorescence (Flu) spectra of the CP43 complex at 77 and 293 K (Abs) calculated with the site energies in Table 1 are compared with experimental data.[37] The calculations are shown as lines and the experimental data as symbols.

Table 1. Site Energies and Corresponding Wavelengths in the CP43 Complex, Optimized by a Fit of the Linear Optical Spectra in Figure 1[a]

Chl	33	34	35	**37**	41	42	**43**
$(E/hc)/\text{cm}^{-1}$	14993	14859	14925	**14749**	15129	14925	**14793**
λ/nm	667	673	670	**678**	661	670	**676**
Chl	44	**45**	46	47	48	49	
$(E/hc)/\text{cm}^{-1}$	14859	**14793**	15038	15038	14925	14993	
	673	**676**	665	665	670	667	

[a] The three Chls with the lowest site energies and the respective values are highlighted.

Stationary Spectra of CP43 and CP47. A genetic algorithm, described previously,[35,48] was used to determine site energies of the Chls in the CP43 and CP47 subunits from a fit of their linear optical spectra. In Figure 1, the linear absorption, linear dichroism, and fluorescence spectra of the CP43 complex at 77 K, calculated for the optimized site energies in Table 1 , are compared with experimental data.[37] From the temperature dependence of the absorption spectrum in the upper part of Figure 1, a Huang−Rhys factor $S \approx 0.5$ is inferred, which is comparable in magnitude to the $S = 0.65$ estimated for the reaction center pigments previously.[35] A width $\Delta_{inh} = 180 \text{ cm}^{-1}$ (fwhm) of the Gaussian distribution function for the site energies gave the best fit. The same $S = 0.5$ and $\Delta_{inh} = 180 \text{ cm}^{-1}$ are used for the Chls in CP47, because both core antenna subunits have similar structures. The optical spectra of the CP47 complex, calculated with the optimized site energies in Table 2, are compared in Figure 2 with experimental data at 77 K (linear absorption and linear dichroism,[38] fluorescence[39]) and at 293 K (circular dichroism[40]).

The wavelengths corresponding to the site energies in Tables 1 and 2 vary between 661 and 688 nm. The three lowest site

Table 2. Site Energies and Corresponding Wavelengths in the CP47 Complex, Optimized by a Fit of the Linear Optical Spectra in Figure 2[a]

Chl	**11**	12	13	14	15	16	17	21
$(E/hc)/\text{cm}^{-1}$	**14684**	15060	14793	14950	14810	14880	15130	14970
λ/nm	**681**	664	676	669	675	672	661	668
Chl	22	23	**24**	25	26	27	28	**29**
$(E/hc)/\text{cm}^{-1}$	14810	15270	**14710**	15060	14860	14880	14970	**14530**
λ/nm	675	655	**680**	664	673	672	668	**688**

[a] The three Chls with the lowest site energies and the respective values are highlighted.
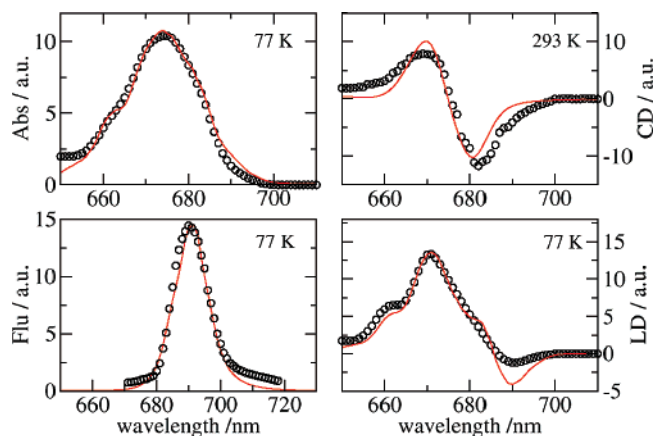

Figure 2. Absorption (Abs), circular dichroism (CD), fluorescence (Flu), and linear dichroism (LD) spectra of the CP47 complex at 77 K (Abs, Flu, LD) and 293 K (CD), calculated with the site energies in Table 2 are compared with experimental data for Abs and LD,[38] Flu,[39] and CD.[40] The calculations are shown as lines and the experimental data as symbols.
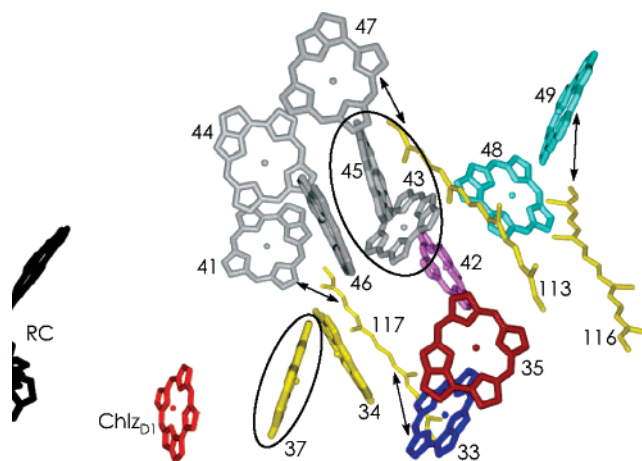

Figure 3. Arrangement of pigments in the CP43 complex. The pigments are numbered as in ref 3. Chls with the same color belong to the same exciton domain. A cutoff energy of 36 cm^{-1} was used in the definition of the domains. If two pigments are coupled stronger than this value, they belong to the same domain. Arrows indicate a van der Waals contact between the conjugated π-systems of a carotenoid and a Chl. The three encircled Chls are those with the lowest site energies (trap states). In addition, a small part of the reaction center including Chlz$_{D1}$ is shown. The figure was prepared with program DINO (http://www.dino3d.org).

energies in CP43 belong to Chls 37, 43, and 45 (using the numbering of Loll et al.[3]), whereas the low-energy pigments in CP47 are Chls 11, 24, and 29. The low-energy Chls in CP43 are located relatively close to the RC as seen in Figure 3, whereas those of CP47 are distributed over the whole complex (Figure 4).
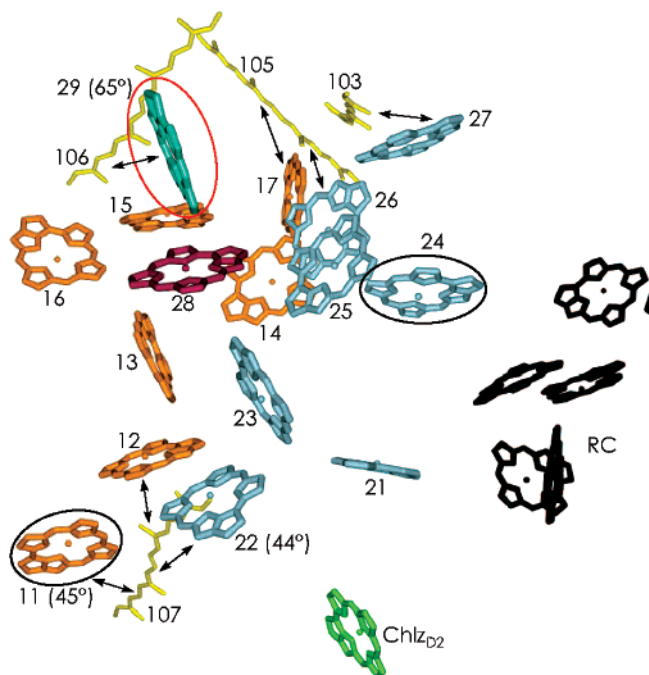
Figure 4. Arrangement of pigments in the CP47 complex. The pigments are numbered as in ref 3. Chls with the same color belong to the same exciton domain. A cutoff energy of 36 cm^{-1} was used in the definition of the domains. If two pigments are coupled stronger than this value, they belong to the same domain. Arrows indicate a van der Waals contact between the conjugated π-system of a carotenoid and a Chl. The three encircled Chls are those with low site energies (trap states); the one with the lowest site energy is encircled in red. Angles of Chl transition dipoles with respect to the membrane plane that are larger than 35° (corresponding to θ < 55°) are shown in parentheses. In addition, part of the RC including Chlz$_{D2}$ is shown. The figure was prepared with program DINO (http://www.dino3d.org).

Chl 24 is the only low-energy Chl of CP47 that is close to the RC. Two of the low-energy pigments in CP43 (Chls 43 and 45) are part of a large exciton domain of six strongly coupled Chls and one, Chl 37, forms a dimer domain with Chl 34. In CP47 all three low-energy pigments are located in different domains. Two of them, Chls 11 and 24, are part of large domains, each containing seven Chls, in the lumenal and stromal layer, respectively, and Chl 29 has a localized excited state. It is the red-most pigment in the whole PS-II core complex and gives rise to a negative LD signal at low energies (long wavelengths).

We note that including the nonconservative experimental CD spectrum of CP43 in the genetic fit of the site energies did not give convergent results. As noted earlier, the present exciton theory cannot describe a nonconservative CD signal. The deviations between the CD spectrum calculated for the present site energies, optimized without CD, and the experimental CD spectrum are significant; a comparison is shown in the SI (Figure 1).

Time-Resolved Spectra of CP43 and CP47. The site energies of the CP43 and CP47 subunits determined above from the fit of stationary spectra together with the Huang−Rhys factor $S = 0.5$ and the inhomogeneous width $\Delta_{inh} = 180$ cm^{-1} for the distribution function of site energies were used to calculate time-resolved pump−probe spectra. In Figures 5 and 6 the pump−probe signals calculated for different probe wavelengths and delay times after excitation by a 60 fs pump pulse centered at 671 nm (CP43) or 670 nm (CP47) are compared with experi-
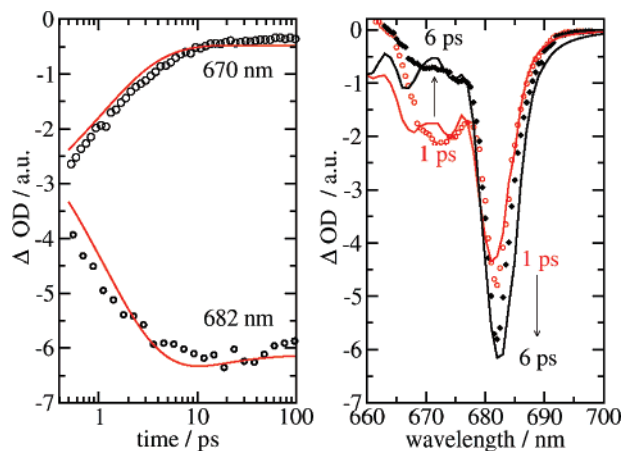

Figure 5. 77 K pump−probe spectra of the CP43 complex, calculated using the site energies and the Huang−Rhys factor from the fit of the linear spectra in Figure 1, are compared with experimental data.[41] The CP43 complex was excited with a 60 fs pump−pulse, centered at 671 nm. The left part of the figure contains the pump−probe signal at two different probe wavelengths dependent on the delay time between the pulses and the right part the pump−probe spectra at two different delay times. The experimental data are shown as symbols and the calculations as solid lines.
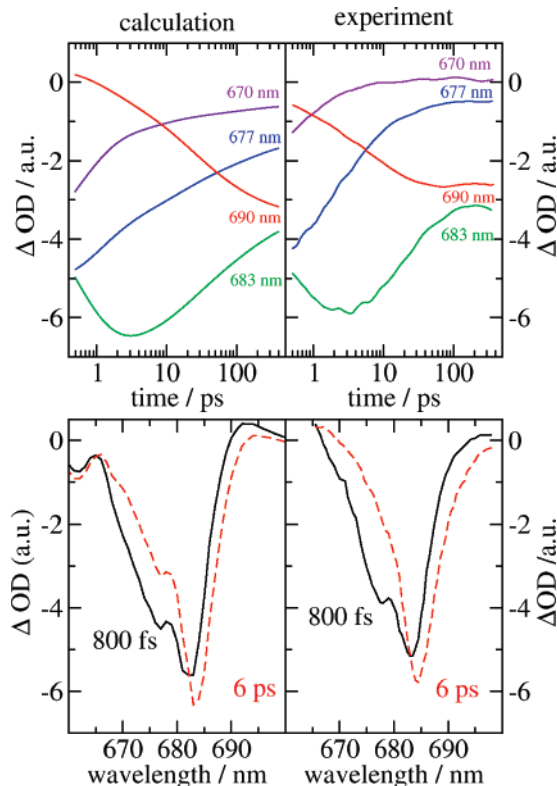

Figure 6. 77 K pump−probe spectra of the CP47 complex calculated using the site energies from the fit of the linear spectra in Figure 2 are compared with experimental data. The CP47 complex was excited with a 60 fs pump−pulse, centered at 670 nm. The upper part of the figure contains the pump−probe signal at four different probe wavelengths dependent on the delay time between the pulses and the lower part the pump−probe spectrum for two different delay times. The calculations are shown on the left and the experimental data on the right.

mental data.[41] In the case of CP43, quantitative agreement between calculated and measured spectra is obtained. The pump−probe signal reflects exciton transfer/relaxation from high to low energies that occurs on a sub-picosecond and picosecond time scale and is finished in about 6 ps. In CP47, in addition to these fast components, there are longer relaxation times detected
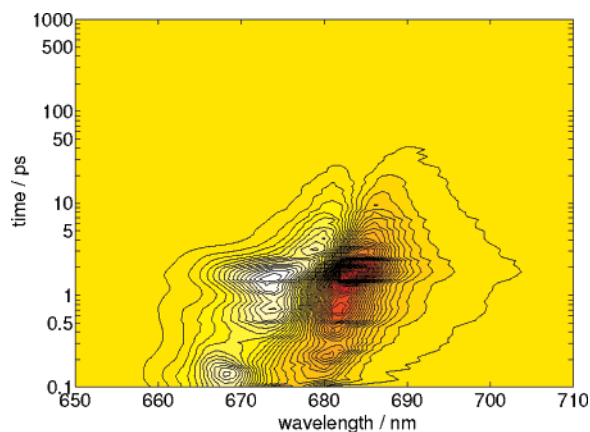
Figure 7. Lifetime density map of time-dependent emission of the CP43 complex at 77 K, calculated by assuming excitation with a 60 fs pulse at 671 nm.
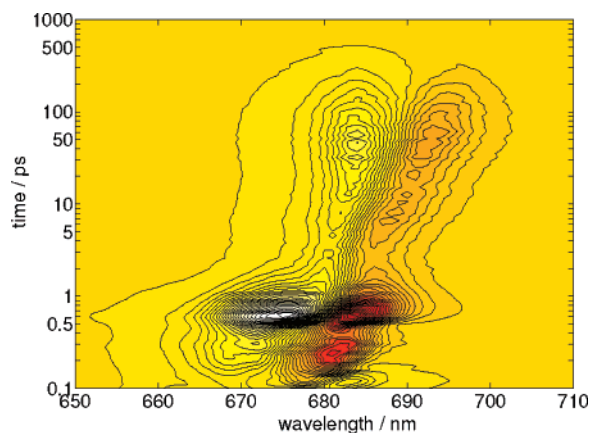

Figure 8. Lifetime density map of time-dependent emission of the CP47 complex at 77 K, calculated by assuming excitation with a 60 fs pulse at 670 nm.

and calculated in Figure 6. These slow processes last until about 100 ps in the experiment and somewhat longer in the calculations. Except for these deviations, there is a good qualitative agreement between the calculated and measured spectra for CP47. The exciton relaxation processes in CP43 and CP47 and their relative amplitudes are illustrated in the LFD maps of time-dependent emission in Figures 7 and 8.

In CP43, there are two main relaxation components of about 200 fs and 2 ps. In CP47, besides the two main components of 250 and 700 fs, dispersive decay behavior is calculated with time constants ranging from 5 to 100 ps. The latter changes qualitatively at room temperature. A main slow component at 10 ps appears, whereas the faster components are not changed qualitatively (SI, Figure 2).

Time-Dependent Fluorescence of PS-II Core Complexes. The site energies, determined from the linear spectra and tested in the simulations of nonlinear spectra, were applied to calculate the time-dependent fluorescence of PS-II core complexes at 300 K. The experimental frequency-integrated and time-resolved fluorescence,[11] detected after excitation with a 100 fs optical pulse that was centered at 663 nm, can be described by assuming an intrinsic rate constant for primary charge separation of k_{intr} = (100 fs)$^{-1}$, as seen in Figure 9. At times larger than 150 ps the calculated signal falls below the experimental one. This discrepancy at long times is due to the neglect of charge recombination reactions as discussed in the SI (Figure 3).
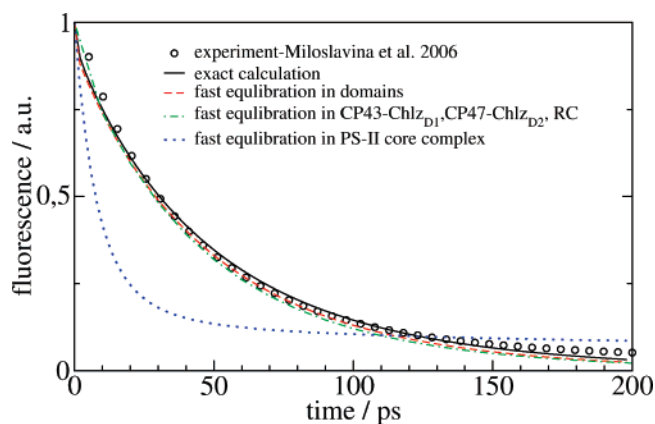
Figure 9. Frequency-integrated fluorescence decay of PS-II core complexes at 300 K calculated in different models, compared to experimental data. The PS-II core complex was excited with a 100 fs optical pulse, centered at 663 nm. The experimental data were reconstructed from Table 1 of ref 11.

To find the bottleneck for the decay of excited states, the fluorescence decay was calculated in simplified models, in which fast equilibration of excitation energy in certain compartments is assumed. The fluorescence decays obtained in these models are compared in Figure 9 with the full calculation and the experimental data. If fast exciton relaxation is assumed in the domains of strongly coupled Chls, virtually the same result as in the calculation without this assumption is obtained for the fluorescence decay (the red dashed and black solid curves in Figure 9). The respective inverse disorder averaged rate constants $\langle k_{a \to b} \rangle_{dis}^{-1}$ (with the $k_{a \to b}$ in eq 33) in Figure 10 show that the fastest transfer between exciton domains in different layers in CP43 and CP47 occurs with time constants of 2–7 ps at 77 K and room temperature. The disorder average $\langle ... \rangle_{dis}$ was performed with respect to the site energies of the pigments, in the same way as for the optical spectra, explained below eq 9. If fast exciton relaxation is assumed in the whole CP43, CP47, and RC subunits, there are still only very minor deviations with respect to the complete calculation, as seen in Figure 9. Because Chlz$_{D1}$ equilibrates more rapidly with CP43 than with the RC and, similarly, Chlz$_{D2}$ with CP47, these two Chlz were included in the compartment of the respective antenna subunit.

The disorder averaged inverse rate constants for this three-compartment model and a five-compartment model, where the Chlz are in separate compartments, are shown in Figure 11. The intercompartment rate constants were obtained from eq 35 and averaged over disorder in site energies. The time constant for exciton transfer between the CP47–Chlz$_{D1}$ compartment and the RC at room temperature is 50 ps and that between CP43–Chlz$_{D2}$ and the RC is 41 ps. If fast exciton equilibration in the whole PS-II core complex is assumed, as in the ERPE model, large deviations with respect to the complete calculation are obtained (the blue dotted and black solid lines in Figure 9).

An analysis of the excitation energy transfer and trapping dynamics in PS-II core complexes is given in Figure 12 by means of the fluorescence LFD map, calculated either with or without electron transfer (including charge recombination reactions). The LFD map without electron transfer was calculated to analyze the time constants of exciton relaxation/transfer in the system. Several components ranging from sub-picoseconds to 200 ps are found (components A–F in Figure 12). These components reflect intradomain exciton relaxation (A, B), exciton transfer
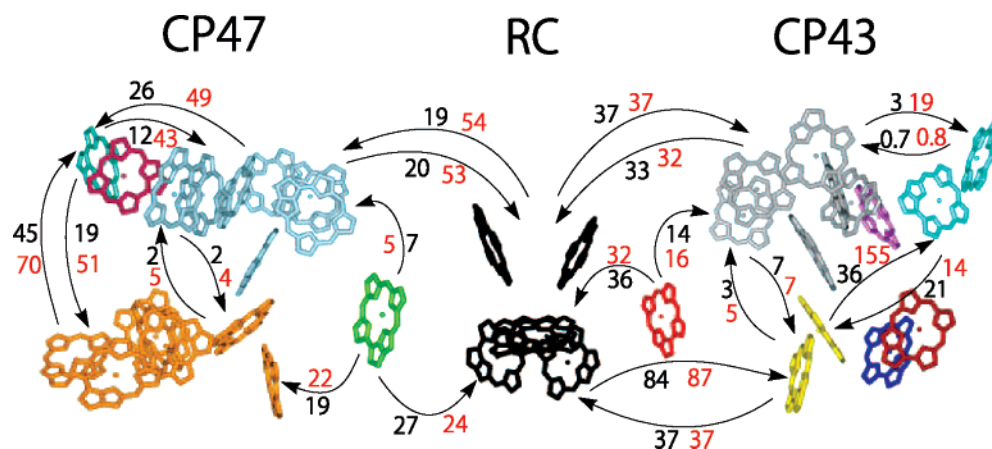
Figure 10. Disorder-averaged inverse rate constants in units of picoseconds for important transfer paths between exciton domains in the PS-II core complex, assuming fast intradomain exciton relaxation, at 300 K (black numbers) and 77 K (red numbers). Chls with the same color belong to the same exciton domain.
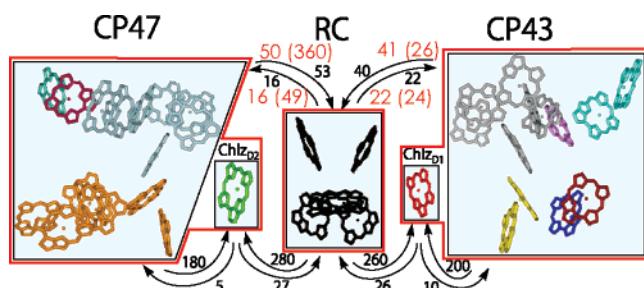

Figure 11. Disorder-averaged inverse rate constants in units of picoseconds for exciton transfer between compartments in the PS-II core complex assuming fast intracompartment exciton relaxation. The numbers in black refer to a five-compartment model, containing CP43, CP47, RC, $Chlz_{D1}$, and $Chlz_{D2}$ for $T = 300$ K. The numbers in red were obtained for a three-compartment model with the compartments CP43−$Chlz_{D1}$, CP47−$Chlz_{D2}$, and RC at $T = 300$ K and 77 K (numbers in parentheses).

Figure 12. Lifetime density maps of time-dependent emission of PS-II core complexes calculated with and without electron transfer, assuming excitation by a 100 fs pulse at 660 nm, $T = 300$ K.

between the domains in one subunit (B), exciton transfer to the trap state of CP47 and exciton equilibration between CP43, CP47, and RC (C), exciton transfer between CP43 and CP47 via the RC (D), exciton transfer from CP43 to RC and CP47 to RC and trapping in the RC (E), and electron transfer between RP2 and RP3 and recombination (F).

The disorder averaged inverse rate constants in Figure 11 show that at room temperature excitation energy transfers
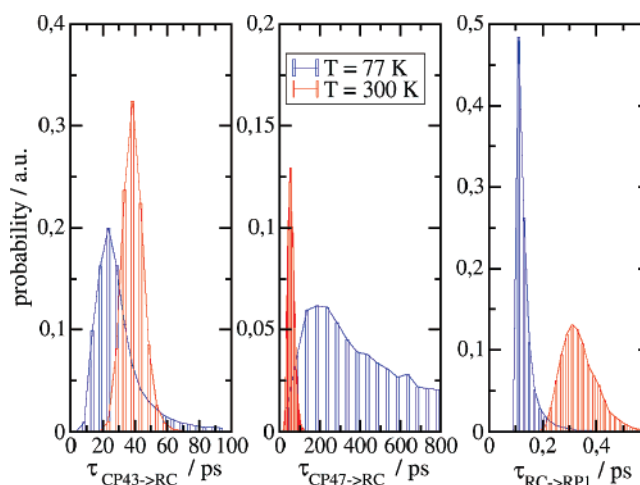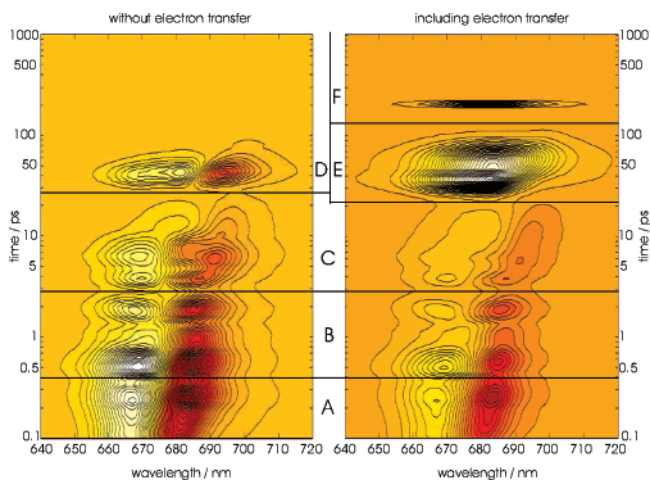

Figure 13. Probability distribution of time constants for transfer from CP43 to RC (left) and from CP47 to RC (middle) and primary electron transfer (right) at $T = 77$ K (blue) and $T = 300$ K (red). The rate constants were obtained in the three-compartment model; that is, $Chlz_{D1}$ was included in the CP43 compartment and $Chlz_{D2}$ in that of CP47.

between CP47 and RC and between CP43 and RC occur with similar time constants of 40−50 ps. However, at 77 K a striking decrease of the rate constant $k_{CP47 \rightarrow RC}$ is obtained: It slows by an order of magnitude (red numbers in parentheses in Figure 11). To understand the origin of this temperature dependence, the probability distributions of the different time constants were calculated, including also the time constant $\tau_{RC \rightarrow RP1} = (k_{RC \rightarrow RP1})^{-1}$ (eq 34) for primary electron transfer. As shown in Figure 13, the maxima of the distribution functions of the time constants of the primary electron transfer and excitation energy transfer between CP43 and RC move toward shorter times at 77 K, but their widths do not change qualitatively.

In contrast, the rate of excitation energy transfer from CP47 to the RC (middle panel in Figure 13) at 77 K becomes highly dispersive, the width of the distribution of the respective time constant increases by an order of magnitude, and the maximum shifts from 50 ps at 300 K to 200 ps at 77 K. If the site energy of Chl 29 in CP47 is increased such that the corresponding wavelength decreases from 688 to 670 nm (which corresponds to the site energy of the equivalent Chl 49 in CP43), a large part of the dispersive behavior is lost, as seen in Figure 14 (red curve) and the average time constant for transfer from CP47 to
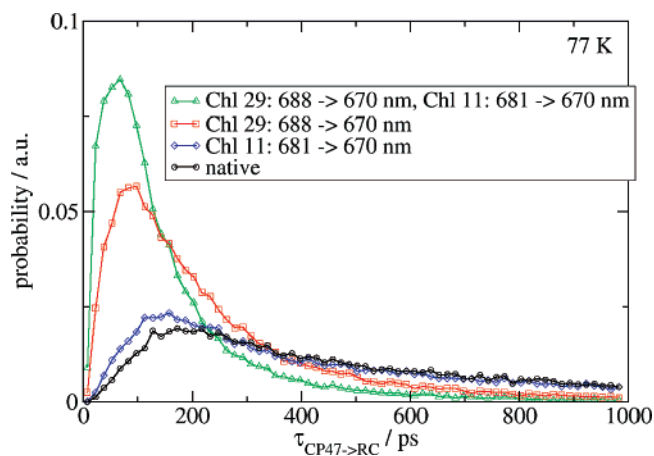
Figure 14. Probability distribution of time constants for transfer from CP47 to RC at $T = 77$ K for the native system (as in Figure 13, middle part) compared to that for modified systems in which the site energies of two trap states were increased as indicated in the figure.
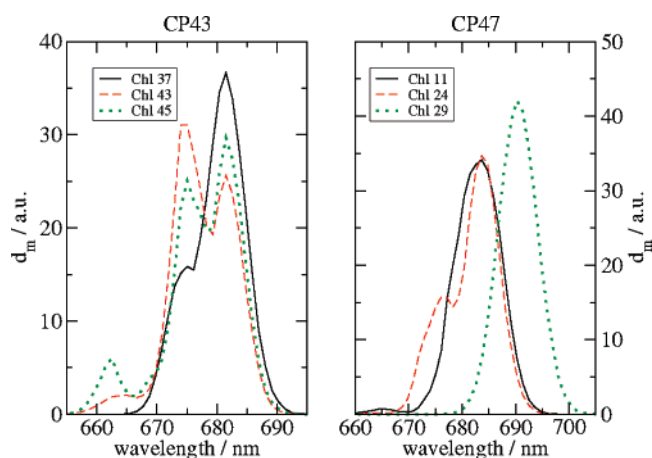

Figure 15. Exciton state pigment distribution function $d_m(\omega)$ (eq 42) for the three low-energy pigments in CP43 (left) and CP47 (right).

the RC decreases from 400 ps in the native system to 100 ps in the modified system. Increasing the site energy of a different CP47 trap state, the one at Chl 11, which is also located at a large distance to the RC, has only a minor effect on the transfer efficiency to the RC (the blue line in Figure 14). However, up-shifting the site energies of both these CP47 trap states results in a cooperative effect; that is, the maximum of the distribution function for the CP47 → RC transfer times shifts furthest toward shorter times (the green line in Figure 14).

Discussion

Trap States in CP43 and CP47. For the analysis of the antenna trap states, the exciton-state pigment distribution function

$$d_m(\omega) = \left\langle \sum_M |c_m^{(M)}|^2 \delta(\omega - \omega_{M0}) \right\rangle_{dis} \qquad (42)$$

introduced previously[35] is shown in Figure 15 for the three pigments with the lowest site energies in CP43 and CP47 (compare Tables 1 and 2). Whereas in CP43 all three low-energy pigments contribute at the lowest excitation energy of the sub-unit, in CP47 just Chl 29 has a contribution. In addition, all of the functions d_m except for the one of Chl 29 indicate a certain

delocalization of the excitons by multiple maxima or at least shoulders.

In CP43, two of the three pigments, Chls 43 and 45, belong to the same domain, whereas Chl 37 is part of a dimer domain with Chl 34 (see Figure 3). Hence, there are two degenerate low-energy exciton transitions around 682 nm that represent the lowest excited states of the two domains in the lumenal (containing Chls 34 and 37) and stromal layers (containing Chls 41 and 43−47). These characteristics fit very nicely to the A- and B-states identified in NPHB and triplet bottleneck spec-trs[37,43,44] discussed in the Introduction. The B-state is identified as the low-energy exciton state of the stromal domain with six pigments (shown in gray in Figure 3), whereas the A-state is the low-energy exciton state of the Chl 34−37 dimer on the lumenal side (shown in yellow in Figure 3). Whereas there is a van der Waals contact between Chls and carotenoids for Chls 41 and 47 of the large domain, there are no such connections for Chls 34 and 37 in the dimer. This difference could be why the A-state does show a strong triplet bottleneck signal and the B-state does not.[43] The hydrogen bonds predicted by Groot et al.[37] on the basis of the vibrational fine structure of the emission most likely are formed between the 13^1-keto group of the low-energy Chls 43 and 45 of the B-state domain and His C164 and Ser C275, respectively.

Concerning the larger hole burning efficiency of the B-state, at first glance, both explanations discussed in the Introduction could apply. Because the B-state domain is 3 times larger than the dimeric A-state domain, it can collect more excitation energy, as suggested by Jankowiak et al.[43] On the other hand, the hydrogen bonds to Chls 43 and 45, discussed above, could explain the higher photoconversion of the B-state, as proposed by Krausz and co-workers,[44] because no such hydrogen bonds exist for Chls 34 and 37 in the A-state domain. As seen in Figure 10, both layers of the membrane are well connected by excitation energy transfer. Hence, the present calculations are in favor of the proposal of Krausz and co-workers.[44] A possible explanation of the narrow 0−0 line shape measured in hole burning[43] is that at low temperature those complexes are selected from the ensemble in the sample which have nondegenerate low-energy exciton states and where the energy gap between the two antenna trap states (A and B) is large compared to the thermal energy. In this case, the excited states of the pigments in the exciton state with the lowest energy have a long lifetime and therefore exhibit a high hole burning efficiency.

The coupling between the A-state Chls 37 and 34 is seen as a shoulder of the function d_{37} in Figure 15 around 672 nm. In the experiment this shoulder is found at somewhat shorter wavelengths (higher energies) around 669 nm,[37,43] indicating that the site energy of Chl 34 might be slightly higher than determined here from a fit of the linear spectra. Concerning the excitonic coupling in the B-state domain, Jankowiak et al.[43] found correlations between the B-state at 683 nm and other exciton transitions at 678 and 673 nm. The correlation between 683 and 673 nm involve Chls 43 and 45, as shown in Figure 15.

In agreement with de Weerd et al.,[38] the present calculations show that the lowest excited state of CP47 is localized on a monomeric Chl, namely, Chl 29. From the 16 Chls in CP47 only Chls 11, 22, and 29 have an angle between their transition dipole moment and the membrane plane larger than 35° and

therefore could be responsible for the negative LD signal observed at low energies. Chls 11 and 22 are part of two large exciton domains in the lumenal and stromal layers of the membrane, respectively. Hence, the only localized excited state with negative LD is the one of Chl 29.

The 2 nm blue shift of the low-temperature fluorescence that occurred after mutation of His B114,[46] which turned out to be the axial ligand of Chl 29,[3] to Gln provides further support for the present assignment. Chl 29 forms a hydrogen bond to Thr H5 of the H-subunit, in agreement with the prediction of a strong hydrogen bond of the low-energy Chl from the FLN spectra.[38] The absence of a 690 nm bleaching in the T−S signal[38] could very well be due to the quenching of the triplet energy of Chl 29 by Car 106 (see Figure 4). From the three low-energy pigments in CP47, only Chl 24 is not in van der Waals contact with a carotenoid. Therefore, it can be expected to be the main contributor to the T−S signal. As suggested from anisotropy measurements,[38] the 683 nm state consists of more than one exciton transition. Chls 11 and 24, which are located in different domains (see Figure 4), contribute to different exciton transitions at this wavelength (Figure 15).

Excitation Energy Transfer in the CP43 and CP47 Subunits. The experimentally found 0.2−0.4 and 2−3 ps time constants[41] for exciton relaxation in CP43 complexes are well reproduced by the calculations of the pump−probe spectra in Figure 5 and the LFD map in Figure 7. As described above, there are two trap states in CP43, one in the lumenal layer and one in the stromal layer. The 200 fs time constant reflects exciton relaxation in the domains and exciton transfer between the domains in the same layer to the trap state domain. As seen in Figure 10, the disorder averaged transfer times between the trap state domain in the stromal and the one in the lumenal layer are 5 and 7 ps at T = 77 K, which appear to be somewhat too slow to explain the main 2 ps equilibration time constant in the LFD map in Figure 7. The latter is understood by taking into account, instead of the average value, the maxima of the probability distribution of these time constants, which are both about 4 ps (SI, Figure 4). The resulting 2 ps equilibration time explains also the pump−probe spectra in Figure 5.

The LFD map of CP47 in Figure 8 contains strong 500−800 fs components that appear to be somewhat too fast for exciton relaxation between the lumenal and stromal layers as judged by the disordered averaged transfer times in Figure 10, which would yield a relaxation time of about 2 ps. As in the case of CP43, the distribution of this interlayer transfer time in CP47 is asymmetric (data not shown). If one uses the maxima of the distributions, one arrives at an equilibration time of about 1 ps, which is still slightly too slow to explain the fast components in the LFD map. Obviously, the latter are dominated by contributions from intradomain exciton relaxation to the degenerate 683 nm trap states in each of the two domains in the lumenal and stromal layer. From these two trap states a largely dispersive transfer to the 690 nm trap state at Chl 29 occurs with time constants that have a strongly asymmetric distribution at 77 K with maxima in the 20−60 ps range. This behavior is reflected in the measured and calculated pump−probe signal in Figure 6. The 683 nm signal first becomes more negative up to a delay time of 2 ps and then starts to increase up to 100 ps in the experiment and somewhat longer in the calculations. The rise of the negative signal reflects excitation energy transfer to

the 683 nm trap states and, therefore, increased SE at this wavelength. The decay of this signal at larger times and the parallel growth of the negative signal at 690 nm are due to excitation energy transfer to the trap state at Chl 29.

Excited-State Decay in PS-II Core Complexes. Having determined the site energies from linear optical spectra and having tested them in the calculation of time-resolved spectra provide a solid ground to investigate excitation energy transfer and trapping in PS-II core complexes. The measured main 40−50 ps decay component of the fluorescence[11] can be described only by assuming that charge recombination reactions occur on a slower time scale. Assuming a faster recombination would cause a too slow decay of the fluorescence in contradiction with the experimental data. This finding enables one to describe the decay by using only one adjustable parameter, namely, the k_{intr} for primary electron transfer. A quantitative description of the experimental data is obtained in Figure 9 for $k_{intr} = 100$ fs^{-1}. Due to the partial delocalization of exciton states in the RC and the fast equilibration of exciton-state populations prior to electron transfer, the first radical pair state is created with a time constant of about 300 fs, as seen in the right part of Figure 13 (see also eqs 31 and 34).

This time constant is an order of magnitude faster than the 3 ps inferred from pump−probe spectra in the visible spectral range[12] and about a factor of 2 faster than the 600−800 fs from mid-IR−vis pump−probe data[16] on D1−D2−cyt*b*559 complexes. If real, the discrepancy by a factor of 2 between the latter result and the present calculations might reflect a conformational difference between D1−D2−cyt*b*559 and PS-II core preparations that could change the electron-transfer coupling matrix element between Chl$_{D1}$ and Pheo$_{D1}$ or lead to a slight change of the driving force of the reaction. In fact, a 4 nm red shift of the site energy of Chl$_{D1}$ in PS-II core complexes as compared to that in D1−D2−cyt*b*559 complexes was found,[36] which could have the same origin. On the other hand, using an intrinsic rate constant of $k_{intr} = 200$ fs^{-1} that corresponds to a Pheo reduction with a time constant of 600 fs, as reported in ref 16, results only in a slightly less satisfying description of the measured fluorescence decay (SI, Figure 5). However, the present model is not consistent with a time constant of 3 ps[12] for Pheo reduction (SI, Figure 5).

In bacterial reaction centers, electron transfer starting at the accessory bacteriochlorophyll was found to occur an order of magnitude more quickly (<400 fs) than electron transfer starting at the special pair (3 ps).[56,57] Taking into account the high similarity in arrangements of Chl$_{D1}$ and Pheo$_{D1}$ and its bacterial counterparts (a detailed comparison is given in ref 36), the present finding of ultrafast primary electron transfer provides further support for Chl$_{D1}$ as the primary electron donor in PS-II.

The direct detection of the ultrafast intrinsic rate constant of 100 fs^{-1} for primary charge separation, inferred here, is difficult, because it is impossible to excite the primary donor Chl$_{D1}$ exclusively in PS-II core complexes. It would, therefore, be helpful to repeat the earlier experiments on ultrafast electron transfer starting at the accessory bacteriochlorophyll in bacterial reaction centers[56,57] with a higher time resolution to pinpoint

(56) van Brederode, M. E.; Jones, M. R.; van Mourik, F.; van Stokkum, I. H. M.; van Grondelle, R. *Biochemistry* **1997**, *36*, 6855.
(57) van Brederode, M. E.; van Mourik, F.; van Stokkum, I. H. M.; Jones, M. R.; van Grondelle, R. *Proc. Natl. Acad. Sci. U.S.A.* **1999**, *96*, 2054.

the exact value of this rate constant. In the present treatment, k_{intr} was just treated as a fit parameter without using any mechanistic description of the electron-transfer reaction. The assumed dependence of $k_{M \to RP1}$ on $|c_{Chl_{D1}}^{(M)}|^2$ in eq 31 seems to suggest a second-order perturbation theory in the electronic coupling, that is, a non-adiabatic reaction. However, because of the low site energy of Chl_{D1}, the $|c_{Chl_{D1}}^{(M)}|^2$ is essentially nonzero only for one exciton level that is strongly localized on the primary donor.[35,36] Hence, the square of the coefficient just ensures that primary electron transfer starts at Chl_{D1}^*. The fast time constant of 100 fs for primary electron transfer, inferred here, provides some indications that the electron-transfer reaction occurs beyond the non-adiabatic limit, that is, in a more adiabatic way, where the rate constant is determined by the vibrational motion in an adiabatic surface that reflects a certain delocalization between the initial and the final states of the primary electron-transfer reaction in eq 32.

Indeed, there are some independent experimental facts that point in this direction: (i) Krausz et al.[58] reported experimental evidence about quinone reduction after long wavelength excitation (up to 730 nm) at cryogenic temperatures. A possible explanation of this phenomenon could be that due to the quantum mechanic mixing of Chl_{D1}^* and Chl_{D1}^+ $Pheo_{D1}^-$ the latter state borrows some oscillator strength from the former and therefore can be directly excited.[27] (ii) To explain their unconventional Stark spectra, Frese et al.[59] suggested that the low-energy exciton state in PS-II RCs is mixed with a charge-transfer state. (iii) The temperature dependence of the site energy of Chl_{D1}, inferred from the calculation of optical difference spectra,[36] could reflect a temperature-dependent localization of a mixed excited/charge transfer state.[27]

To find the bottleneck for the decay of excited states in PS-II core complexes, calculations were performed, assuming fast exciton relaxation in certain compartments. The respective inverse rate constants are given in Figures 10 and 11. As seen in Figure 9, the simplest model that still describes the decay of excited states is a three-compartment model, where it is assumed that exciton relaxation in CP43–$Chlz_{D1}$, CP47–$Chlz_{D2}$, and RC is fast compared to the transfer between these compartments. The time constants obtained in a five-compartment model with Chlz in extra domains in Figure 11 show that $Chlz_{D1}$ and $Chlz_{D2}$ in terms of light-harvesting function belong to the CP43 and CP47 subunits, respectively, rather than to the RC. The transfer times of 50 and 41 ps between CP43(–$Chlz_{D1}$) and RC and CP47(–$Chlz_{D2}$) and RC (Figure 11) are found to represent the main decay components of excited states in the LFD map of PS-II core complexes in Figure 12. Because of the 2 orders of magnitude faster primary electron transfer, nearly every excitation that reaches the RC is irreversibly trapped. This result shows that the decay of excited states in PS-II is limited by the transfer to the trap, that is, the RC. Note that the rate constants for excitation energy transfer between the compartments are not free parameters, but are obtained from the individual interdomain rate constants, calculated from a microscopic theory.

In the three- and five-compartment models, primary electron transfer was assumed to start from an equilibrated exciton manifold in the RC. The close agreement in Figure 9 between the full calculation that does not assume such an equilibration of excitons prior to charge transfer and the compartment calculations indicates that exciton relaxation in the RC at 300 K occurs on an ultrafast sub-100 fs time scale. Independent support for this result is obtained by a direct calculation of the lifetimes of exciton states in the RC (SI, Figure 6).

The assumption of a fast equilibration of excited states in the whole PS-II core complex prior to electron transfer leads to large deviations with respect to the calculation without restrictions (Figure 9). These deviations provide additional evidence that the excited-state decay in PS-II is not trap-limited. Charge recombination reactions do not play the dominant role for the main decay component of excited states as assumed in the ERPE model. Nevertheless, there is an influence on a longer time scale as seen in Figure 9, where the neglect of charge recombination causes the deviations between the calculated and measured data at 150 ps and longer times. Including charge recombination removes this deviation (SI, Figure 3) and leads to an additional decay component that is seen in the LFD map in Figure 12 at about 200 ps. This time constant is close to the 180 ps transfer time constant[12] assumed in the calculations for the irreversible RP1 → RP3 transfer.

The remaining parameters of the charge recombination model are given in the SI (Figure 4). We note that the minor deviations between the experimental data and the calculations without charge recombination reactions in Figure 9 do not allow these parameters to be faithfully determined. We simply adopted values reported in the literature. However, there is an important restriction on the value used for the difference in standard free energy $\Delta G^{(0)}$ between the excited state of the RC from which electron transfer starts and the charge-separated state RP2 = P_{D1}^+ $Pheo_{D1}^-$. According to the present calculations, this $\Delta G^{(0)} = \Delta G_{intr} + \Delta G_{RP1/RP2}$ must be about 175 meV or larger to avoid significant charge recombination. A significantly smaller $\Delta G^{(0)}$ would slow the decay of excited states such that the experimental data could not be described without scaling the excitation energy transfer rate constants. The latter were determined from independent experiments and calculations and therefore cannot be adjusted. From measurements of the recombination fluorescence, values for $\Delta G^{(0)}$ of 110 meV[60] in D1–D2–cyt$b$559 complexes and 170 meV[61] in PS-II core complexes were reported. The latter is very similar to the present estimate and to the $\Delta G^{(0)} = 170-190$ meV determined for the bacterial reaction centers of *Rh. spaeroides* and *Rh. rubrum*.[62]

Although at room temperature the CP43 to RC and the CP47 to RC transfer times are very similar, there are important differences concerning the locations of low-energy exciton states in the two antenna subunits. Whereas in CP43 the trap states in the lumenal layer and the one in the stromal layer are situated close to the RC, that is, tuned for efficient excitation energy transfer, in CP47 the low-energy trap state at 690 nm at Chl 29 is at a great distance from the RC. The different energetics and locations of the trap states in CP43 and CP47 obtained in the present study can be investigated by low-temperature time-

(58) Krausz, E.; Hughes, J. L.; Smith, P.; Pace, R.; Årsköld, S. P. *Photochem. Photobiol. Sci.* **2005**, *4*, 744.
(59) Frese, R. N.; Germano, M.; de Weerd, F. L.; van Stokkum, I. H. M.; Shuropatov, A. Y.; Shuvalov, V. A.; van Gorkom, H. J.; van Grondelle, R.; Dekker, J. P. *Biochemistry* **2003**, *42*, 9205.
(60) Booth, P. J.; Crystall, B.; Giorgi, L. B.; Barber, J.; Klug, D. R.; Porter, G. *Biochim. Biophys. Acta* **1990**, *1016*, 141.
(61) Hillmann, B.; Moya, I.; Schlodder, E. In *Photosynthesis: from Light to Biosphere*; Proceedings of the Tenth International Congress on Photosynthesis; Mathis, P., Ed.; Kluwer Academic Publishers: Dodrecht, The Netherlands, 1995; Vol. 1, pp 603−606. .
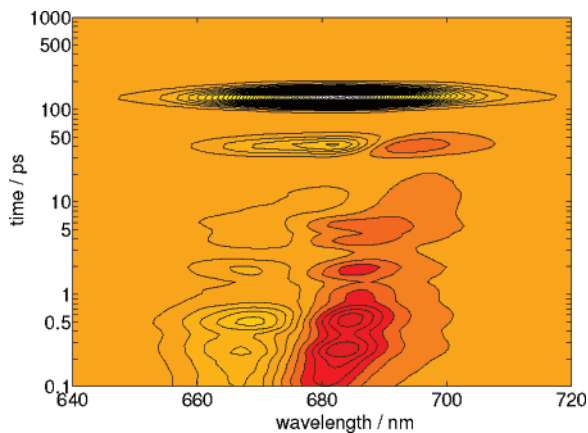(62) Woodbury, N. W.; Parson, W. W. *Biochim. Biophys. Acta* **1986**, *850*, 197.

Figure 16. Lifetime density map of time-dependent emission of PS-II core complexes with closed RCs, assuming excitation with a 100 fs pulse at 660 nm, $T = 300$ K.

resolved spectroscopy. The calculations predict an acceleration of the CP43 to RC transfer at low temperatures and a slowing of the transfer between CP47 and the RC. The latter should become highly dispersive, as seen in Figure 13. Hence, the excited-state decay at 77 K, due to the accelerated CP43−RC transfer, should, on the one hand, contain a 25 ps time constant (Figure 13) that is smaller than the 40−50 ps observed at room temperature and, on the other hand, multiple slower components in the sub-nanosecond range with a maximum amplitude at around 200 ps, as judged from the maximum of the distribution function of the CP47-to-RC transfer time constant in Figure 13. The antenna trap state at Chl 29 in CP47 is mainly responsible for the slow and dispersive transfer from CP47 to the RC at 77 K, as seen in Figure 14. Due to the localized excited state and the low site energy of Chl 29 the excitation energy is efficiently trapped at this site. At low temperatures, the small thermal energy allows only for a slow uphill transfer of the excitation energy from the excited Chl 29 to the exciton states in the neighborhood. The rate constant for this transfer depends critically on the energy differences and therefore varies widely for the different realizations of disorder in site energies, explaining the dispersive nature of the transfer.

A slower fast component of fluorescence decay, by about 3 times, in closed RCs (220 ps) compared to open RCs (80 ps) was measured.[8] This variable fluorescence for open and closed reaction centers was explained in the ERPE model by assuming that the extra electron on the reduced Q_A slows the primary electron transfer by a factor of about 6.[9] In the present model, the variable fluorescence is explained by decreasing k_{intr} from 100 fs^{-1} in open RCs to 6 ps^{-1} in closed RCs, that is, by a factor of 60. In this case, the primary electron transfer converting an excited state of the RC to a charge-separated state takes 18 ps. This time constant now is very similar to those for excitation energy transfer from RC to CP43 (20 ps) and from RC to CP47 (16 ps) (see Figure 11). Hence, an excitation arriving at the RC will be trapped with a probability of one-third compared to a probability of almost one for open RCs, explaining the factor 3 decrease of the fastest time constant in the fluorescence decay for closed RCs seen in the LFD map calculated for closed RCs in Figure 16 compared to that calculated for open RCs in Figure 12.

Because of the smaller trapping probability in closed RCs, excitation energy can be exchanged between CP43 and CP47

via the RC, a process that is not possible for open RCs. As the LFD map calculated without electron transfer in the left part of Figure 12 shows, this transfer takes about 40 ps. Indeed, this energy transfer component is seen in the LFD map for closed RCs in Figure 16. Hence, the present model predicts that an energy-transfer component with a time constant of 40 ps should appear in the time-dependent emission of PS-II core complexes with closed RCs at room temperature.

We note that the time constant detected for the fast fluorescence decay of open RCs has decreased from 80 ps in early experiments[8,9] to 40 ps measured recently.[11] A reason for the discrepancy could be the improved quality of recent PS-II core preparations. It would therefore be helpful to verify whether for recent preparations also a factor of 3 increase in the time constant for the fluorescence decay results upon closing of the RC. We note that the prediction of the present model, concerning the appearance of a 40 ps energy-transfer component, also holds if this factor would be only 2. As for open RCs, also in the case of closed RCs, the decay of excited states in PS-II core complexes can be well described by a three-compartment model as shown in the SI (Figure 7). However, the decay of excited states is not transfer-to-the-trap limited in this case, because the decay is slower by about a factor of 3 than the excitation energy transfer from CP43 or CP47 to the RC.

Under light stress, when the RC is closed, still about one-third of the excitation energy arriving at the RC will be trapped by electron transfer, as discussed above. Because the double reduction of Q_A is a slow process, the charge recombination of $^3[P_{D1}^+ \, Pheo_{D1}^-]$ leads to the formation of $^3Chl_{D1}$ and $^3P_{D1}$. Because of the high oxidative power of the Chls in the RC, no carotenoids are located in their vicinity that could quench the physiologically harmful triplet energy. Instead, in the RC the latter is quenched by Q_A^-.[63,64] The present study suggests that Q_A^-, in addition, redirects the excitation energy back to the antennae with the same goal, namely, the quenching of triplet energy. Chl 29, which has the lowest site energy in the PS-II core complex and is in van der Waals contact with a carotenoid, can be expected to play an important role in this photoprotective process. The importance of Chl 29 for the function of PS-II is also evident from the fact that upon mutation of its axial ligand His B114 to Tyr, PS-II activity is lost.[46]

Conclusions

A set of site energies was provided that describes the stationary and time-resolved spectra of the CP43 and CP47 subunits of PS-II. In particular, the low-energy trap states in these subunits were identified, which are important for light harvesting and photoprotection, because they determine the direction of excitation energy flow and the sites where Chl triplet states form under light stress. On this basis, the decay of excited states in PS-II core complexes was modeled. The main 40−50 ps decay component of excited states measured at room temperature can be described only by assuming that the primary electron transfer is ultrafast and that the free energy difference between the equilibrated exciton states in the RC and the second radical pair state is about 175 meV or larger, so that charge recombination reactions are slow. The calculations demonstrate

(63) Van Mieghem, F.; Brettel, K.; Hillmann, B.; Kamlowski, A.; Rutherford, A. W.; Schlodder, E. *Biochemistry* **1995**, *34*, 4789.
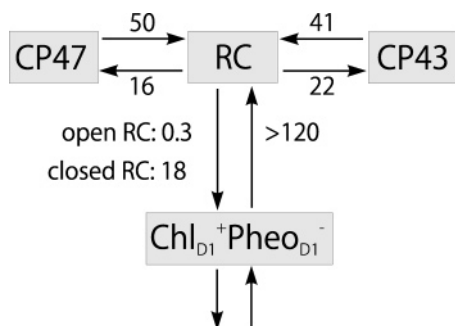(64) Noguchi, T.; *Plant Cell Physiol.* **2002**, *43*, 1112.

Figure 17. Summary of disorder-averaged excitation energy transfer and primary charge-transfer time constants (in units of picoseconds) obtained in the present model. The excitation energy transfer time constants were obtained in the three-compartment model, $T = 300$ K.

clearly that the bottleneck for the decay of excited states in PS-II core complexes with open RCs is due to the transfer from the CP43 and CP47 subunits to the RC; that is, the decay is transfer-to-the-trap limited. The main findings of this paper are summarized in Figure 17, where the minimal three-compartment model is shown with the resulting excitation energy and primary electron-transfer time constants.

The present model suggests a mode switch from a light-harvesting mode for open RCs to a photoprotective mode for closed RCs. For the latter, the rate constant for primary electron transfer slows to an extent that it becomes comparable to the rate for excitation energy transfer from the RC to the core antennae. In this case a considerable part of the excitation energy of the reaction center will return to the antennae and the triplet energy of chlorophyll can be quenched by the carotenoids there. The overall design principle seems to be a RC that is higher in free energy than the antenna, giving rise to fast exit channels for the excitation energy, which are activated only when the RC is closed. This principle is a compromise between high energy-transfer efficiency and photochemical stability of the system.

The following predictions of the present model can be tested by experiments: (i) The main decay component of the fluo-

rescence changes from 40−50 ps at room temperature to 25 ps at 77 K, reflecting faster transfer from CP43 to the RC. In addition, a wide distribution of transfer times with a maximum at 200 ps appears at 77 K, reflecting slower and highly dispersive transfer from CP47. (ii) The fluorescence decay for closed RCs at room temperature contains a 40 ps excitation energy-transfer component that is due to transfer between CP43 and CP47 via the RC.

Of course, a more complete comprehension of the building principles of PS-II core complexes requires a direct calculation of the site energies from structural data. A combined quantum chemical/electrostatic approach was successfully tested on the FMO-protein recently.[34,65] It will be interesting to see whether at the present resolution (3.0 Å) of the crystal structure[3] a similar analysis is feasible for PS-II core complexes.

Supporting Information Available: Derivation of two-exciton shifts, details of line shape functions, excitonic couplings, circular dichroism spectra of CP43, LFD map of time-dependent emission of CP47 at room temperature, influence of charge recombination reactions on fluorescence decay, probability distribution for exciton transfer between the lumenal and stromal trap state domains in CP43, fluorescence decay of open RCs using literature values for k_{intr}, density of states and life times of exciton states in the RC, compartment models for closed RCs. This material is available free of charge via the Internet at http://pubs.acs.org.

JA7099826

(65) Adolphs, J.; Müh, F.; Madjet, M. E.; Renger, T. *Photosynth. Res.* **2008**, *95*, 197.